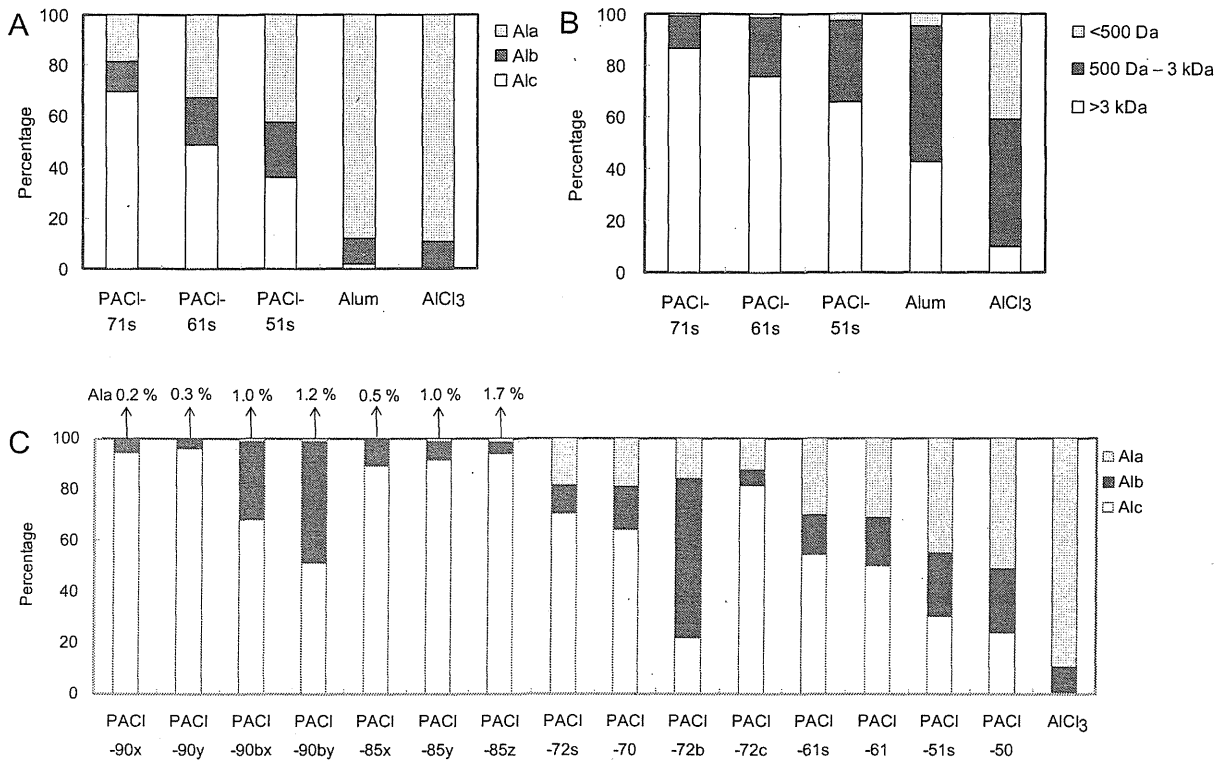

Fig. 1 – Coagulant properties determined by the ferron method (A and C) and membrane filtration fractionation (B). Coagulants in Panels A and B were used for the first set of experiments while those in Panel C were used in the second set of experiments. The standard deviations for the determination of Ala contents (%) were <0.1%.

3.2. *First set of experiments*

3.2.1. *Dissolved residual aluminum and DOC removal in jar tests*

We determined dissolved residual aluminum concentration as a function of coagulation pH for PACl-71s, PACl-51s, $AlCl_3$, and alum (Fig. 2). PACl-71s showed the lowest dissolved residual aluminum concentration at both neutral and weakly alkaline pH, followed by PACl-51s. Yan et al. (2008a) shows that at neutral pH the dissolved residual aluminum concentrations are the same for PACls with different basicities (0–67%), as are the minimum dissolved residual aluminum concentrations attained by adjusting the pH. In contrast, in our study we found that the dissolved residual aluminum concentration decreased with increasing basicity to 71% at both neutral and alkaline pH. In their other data (Yan et al., 2007), 83%- and 73%-basicity PACls shows lower residual aluminum concentration than 53%-basicity PACl even though the coagulation pH values were slightly higher alkaline pH. Therefore, basicity >70% was suggested as a key for reducing residual aluminum concentration.

PACl-71s removed DOC slightly more efficiently than did the other coagulants in both of the tested raw water samples (Fig. 2). Large floc particles were formed with PACl-71s, whereas the floc particles formed with $AlCl_3$ and alum were small at the same dosage (as determined by visual inspection).

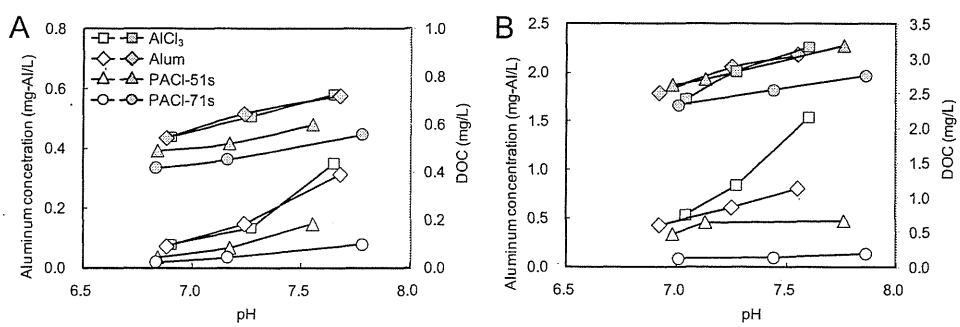

Fig. 2 – Plots of dissolved residual aluminum concentration (open symbols) and DOC (solid symbols) vs. pH for Toyohira River water A with a coagulant dosage of 1.06 mg-Al/L (A) and Chibaberi River water A with a coagulant dosage of 2.12 mg-Al/L (B).

Some investigators have assumed that Al_{13} species (Alb is an index of Al_{13}) are the most effective species for coagulation because they efficiently destabilize particles by means of charge neutralization (Parthasarathya and Buffle, 1985; Gao et al., 2005). On the basis of these previous results, we expected PACl-71s to be the least effective PACl coagulant because it contained the smallest amount of Alb. However, PACl-71s showed the best natural organic matter (NOM) removal. ^{27}Al NMR spectroscopy indicates that commercial PACl products contain less Al_{13} than laboratory-prepared PACls (Lin et al., 2008). However, the coagulation efficiency of commercial PACls is no worse than that of laboratory-prepared PACls (Lin et al., 2008). Recently, Al_{30} polymer, which has been detected among the Alc species and which is formed in processes carried out at high concentrations and temperatures, has attracted attention as an effective coagulant (Chen et al., 2006, 2007, 2009). Because the conditions required for formation of Al_{30} polymer are met by the conditions under which commercial PACl coagulants are prepared, it is possible that some of the species in PACl-71s were structurally similar to Al_{30} polymer. Further study will be required for elucidating the high NOM removals.

3.2.2. *MW distribution of dissolved residual aluminum, as determined by micro and ultrafiltration fractionation*

The data in Fig. 3A–B, for Toyohira River water, indicate that the fraction with a MW range of 0–0.5 kDa was small for all coagulants, which means that most of the dissolved residual aluminum was not in monomeric form. At pH 7.0 for all the coagulants, some of the dissolved residual aluminum was contained in the fraction with a MW range of 0.5–3 kDa. For alum and $AlCl_3$, dissolved residual aluminum was also present in the fraction at 100 kDa–0.45 μm, but aluminum of that MW range was observed at much smaller concentrations for the PACls. Therefore, the lack of colloidal aluminum at 100 kDa–0.45 μm contributed to the overall low concentrations of dissolved residual aluminum observed for the samples after the PACl coagulation. PACl-71s showed a lower dissolved residual aluminum concentration in the fraction at 0.5–3 kDa than did PACl-51s; this further reduced the overall dissolved residual aluminum concentration for PACl-71s relative to that for PACl-51s. These same trends were also observed at pH 7.5.

For Chibaberi River water, which contained a higher NOM concentration than Toyohira water, most of the dissolved residual aluminum was observed in the fraction at 100 kDa–0.45 μm (Fig. 3C–D). The dissolved residual aluminum in this fraction may have been in the form of a soluble aluminum–NOM complex, which exists when the coagulant dosage is insufficient to precipitate all the NOM (Jekel and Henizmann, 1989). The aluminum concentration in this fraction was very low when PACl-71s was used, suggesting that PACl-71s has a smaller tendency to form the soluble aluminum–NOM complex but benefits to form insoluble precipitate Al-NOM. The observed highly efficient removal of NOM by PACl-71s (see Fig. 2) also supports this suggestion. Yan et al. (2007, 2008a) suggested that Ala might form a soluble complex with some types of NOM. If such a soluble complex had a size in the range 100 kDa–0.45 μm, the fact that the aluminum concentration was lowest for PACl-71s could be explained by the fact that PACl-71s had the lowest Ala percentage.

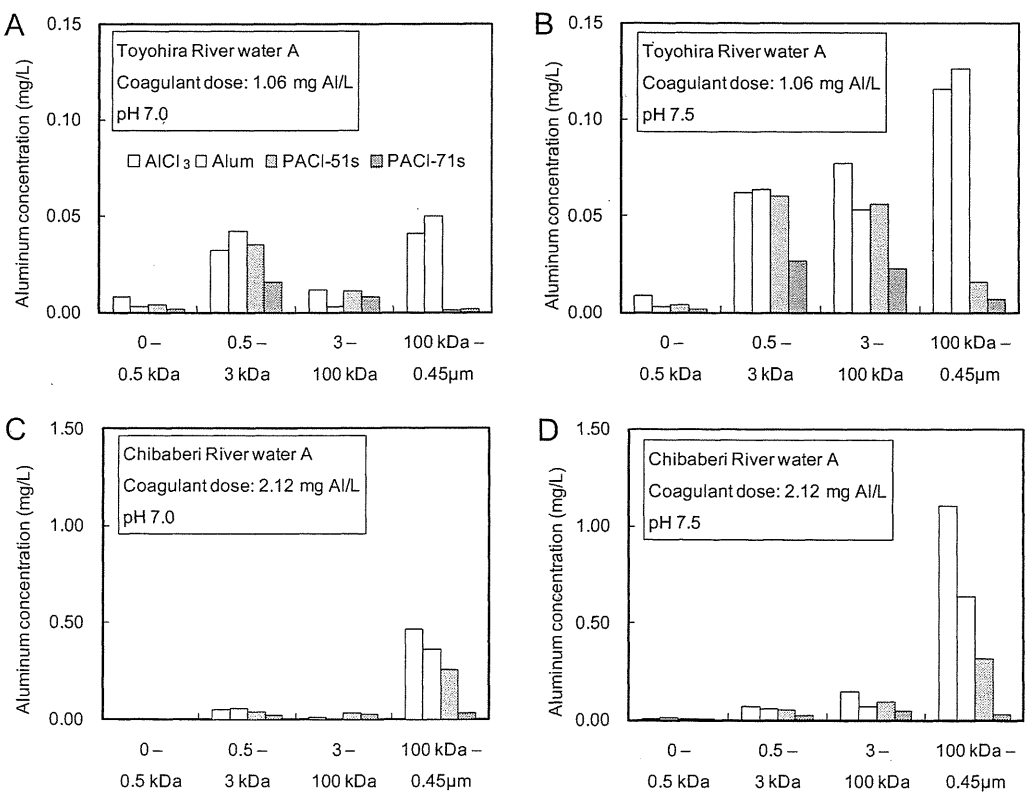

Fig. 3 – MW distribution of dissolved residual aluminum after jar tests, as determined by micro and ultrafiltration fractionation.

3.2.3. *Effect of coagulant dosage on dissolved residual aluminum concentration*

For PACl-51s, the dissolved residual aluminum concentration at pH 7.5 increased with increasing dosage and exceeded 0.2 mg/L at a dosage of 2.12 mg-Al/L (Fig. 1S-B, Supplementary Information). For PACl-71s, no such trend was observed. In all the experiments, PACl-71s removed more DOC than PACl-51s, in agreement with the results described earlier. For PACl-51s treating the other water at pH 7.5, the dissolved residual aluminum concentration approached 0.3 mg/L at the dosage 2.12 mg-Al/L (Fig. 1S-D, Supplementary Information), and almost no turbidity removal was observed (the turbidity of the treated water was 2.0 NTU, whereas that of the raw water was 2.4 NTU; Fig. 2S-D, Supplementary Information). At the same dosage and pH, PACl-71s lowered the dissolved residual aluminum concentration to <0.1 mg/L and lowered the turbidity to 0.4 NTU.

3.2.4. *Effect of water temperature on dissolved residual aluminum concentration*

The influence of water temperature on dissolved residual aluminum concentration was studied with PACl-51s, -61s, and -71s: PACl-61s was selected for these experiments because it has been widely used in commercial water treatment under low-temperature conditions. At high (28 °C) and low (4 °C) temperatures, as well as the standard temperature of 20 °C, PACl-71s reduced the residual aluminum concentration to its lowest levels compared to those obtained for PACl-51s and PACl-61s (Fig. 3S, Supplementary Information). As predicted from the aluminum solubility diagram (Pernitsky and Edzwald, 2003; Geochemist's Workbench, ver. 6, RockWare, Inc., Golden, CO, USA), the higher the water temperature, the higher the residual aluminum concentrations. At pH 7.0, residual aluminum concentrations were almost unchanged between 4 and 20 °C but increased a little at 28 °C. At pH 7.5, the residual aluminum concentrations increased with increasing temperature.

3.3. *Second set of experiments*

To further investigate the low residual aluminum concentrations observed after PACl-71s coagulation, we conducted jar tests with a variety of PACls, including a very-high-basicity PACl (90%), sulfated and non-sulfated PACls, and PACls composed mainly of Alb or Alc (Fig. 1C).

3.3.1. *Effect of sulfate in PACls on dissolved residual aluminum concentration*

As shown Fig. 4A–C, the presence of sulfate ion in PACls did not affect the residual aluminum concentration for pH > 6.5. For pH < 6.5, however, sulfate ions contributed to reducing the residual aluminum concentration. Low residual aluminum concentration, as well as good turbidity removal (Fig. 4S, Supplementary Information), was observed for pH > 7.0 for the non-sulfated PACls, but the pH range for the minimum

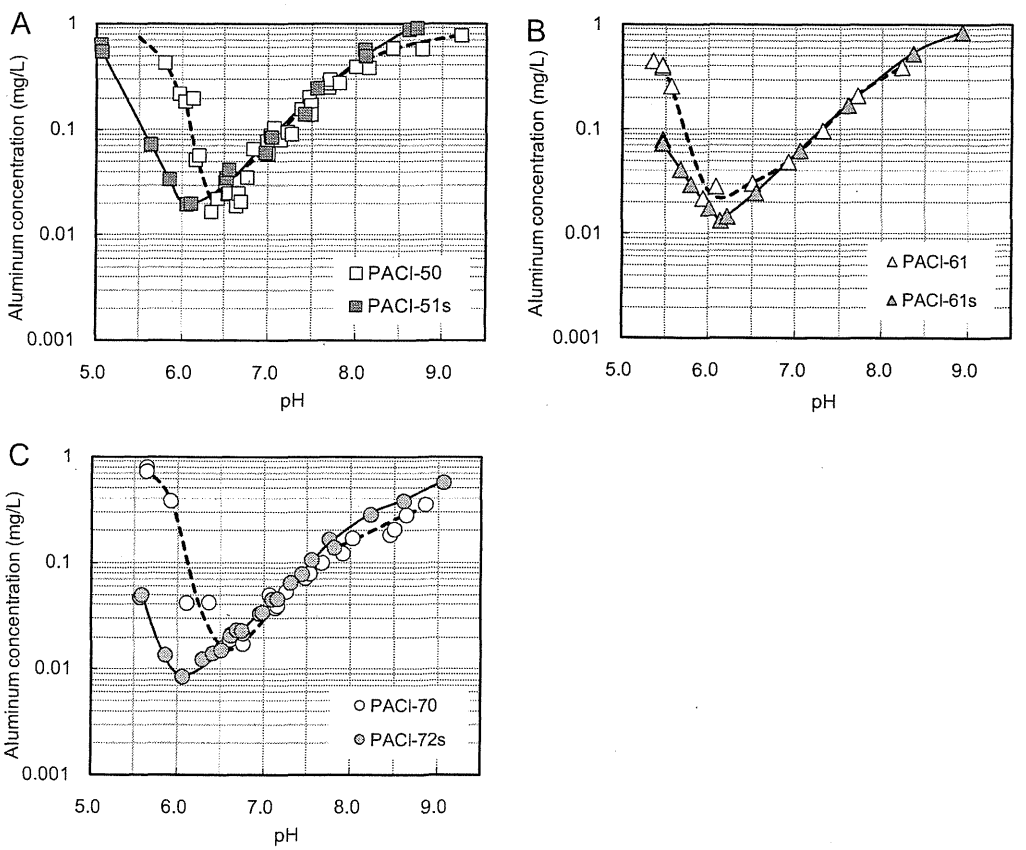

Fig. 4 – Comparison of residual aluminum concentrations between sulfated and non-sulfated PACls(Toyohira River water C, coagulant dosage: 1.89 mg-Al/L).

residual aluminum concentration was shifted to the slightly acidic pH range around 6–6.5 by the presence of sulfate in the PACls. Because sulfate suppresses charge reversal and accelerates the kinetics of aluminum hydroxide precipitation (Amirtharaja and O'Melia, 1990), sulfate is often added to PACls, in particular to effectively treat raw water of low turbidity and low NOM concentrations. In these experiments, we observed that larger floc particles were formed by sulfated PACls than by non-sulfated PACls. The observed lower residual aluminum concentration at acidic pH for sulfated PACls compared to non-sulfated PACls could be due to charge the neutralization effect: the suppression of positively charged polynuclear and microcrystalline hydrolysis products through adsorption and complexation of sulfate (Wang et al., 2002). It should be noted, however, that our results do not agree with those of Pernitsky and Edzwald (2003), who reported that the presence of sulfate did not affect aluminum solubility. They used pure water for comparing aluminum solubility, whereas we used natural waters. Therefore, ionic strength or the presence of other ions in our natural water samples may have affected the residual aluminum concentrations.

3.3.2. *Effects of basicity and polymeric/colloidal species on dissolved residual aluminum concentration*

The effect of the aluminum species (Alb/Alc) on residual aluminum concentration was investigated by comparing the results of PACl-72b and -72c, for which the basicity values are the same but for which the dominant aluminum species are polymeric (Alb) and colloidal (Alc), respectively. Residual aluminum concentrations were almost the same between PACl-72b and -72c at the tested pH range of 5.5–8.5 (Fig. 5A): this data suggests that the residual aluminum concentration was determined by the Ala percentage.

The effect of aluminum species on residual aluminum concentration was further investigated by using a series of PACl coagulants, including the very-high-basicity PACls (PACl-90bx and -90y). As shown in Fig. 5B, aluminum concentrations at pH > 6.5 were the lowest with PACl-90y followed by PACl-90bx and PACl-70. Aluminum concentrations were not largely different between PACl-61 and PACl-50. At coagulation pH of 7.5–8.5, where problematic levels of residual aluminum are generally seen, a residual aluminum concentration <0.02 mg/L was attained with PACl-90y. Good turbidity removal after settling was observed at a coagulation pH of 7.0–8.5 (Fig. 5S, Supplementary Information). Among the PACls, aluminum concentrations decreased with increasing PACl basicity. For sulfated PACls, a similar trend was observed (Fig. 5C). The reason why $AlCl_3$ exhibited a lower aluminum concentration than PACl-50 was not clear, but the results suggest that a basicity ≥70% was required to reduce residual aluminum concentration. PACl-90bx and PACl-90y, in particular, exhibited extremely low residual aluminum: their minimum residual aluminum concentrations were <0.007 mg/L, which was far below the aluminum solubility

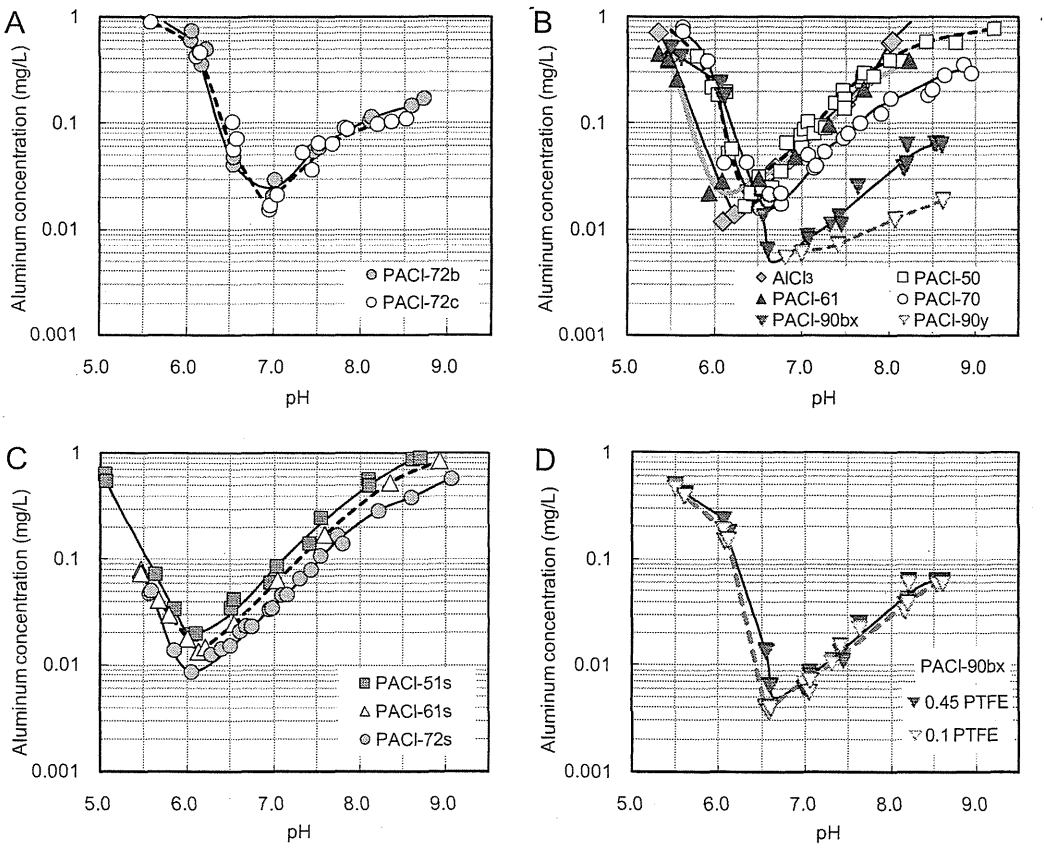

Fig. 5 – Effect of Alb/Alc (Panel A), basicity (Panels B and C), and membrane pore size on residual aluminum concentrations (Panel D) for Toyohira River water C (coagulant dosage: 1.89 mg-Al/L).

reported by Pernitsky and Edzwald (0.03 mg/L; 2003). While concentrations <0.007 mg/L were attained after 0.45-μm membrane filter filtration, residual aluminum concentrations decreased even further, to <0.004 mg/L, when sample water was filtered by a 0.1-μm membrane filter (Fig. 5D).

3.3.3. *Effect of monomeric species on dissolved residual aluminum concentration*

The concentration of residual aluminum observed after PACl-90y coagulation was clearly lower than that after the coagulation by PACl-90bx of the same basicity (Fig. 5B); this discrepancy would be due to the lower Ala perentage in PACl-90y compared with that in PACl-90bx because Alb/Alc ratio did not affect residual aluminum concentration. Therefore, we hypothesized that low Ala percentage, rather than high basicity, was a better indicator for minimizing residual aluminum concentration, although PACl basicity roughly determines the Ala percentage in PACl. The effect of Ala percentage on dissolved residual aluminum was verified by using water samples with high and low NOM concentrations and additional very-high-basicity PACls. Because of the necessity of discussing small differences of Ala percentages, the analytical accuracy of very low Ala percentage was evaluated in multiple measurements for the very-high-basicity PACls. Ala percentages of PACl-90x, 90by, 85x, and 85y were 0.22 ± 0.10, 1.18 ± 0.02, 0.43 ± 0.10, and 1.00 ± 0.07 (avg. ± sd.), respectively: the standard deviations were all <0.1. Fig. 6 shows plots of dissolved residual aluminum concentration against Ala percentage. Among the three PACls with a basicity of 85% (circles in the figure), dissolved residual aluminum concentrations increased with increasing Ala percentage in the order of PACl-85x (Ala: 0.5%) < PACl-85y (1.0%) < PACl-85z (1.7%) (Fig. 6A). A similar trend was also seen for the three PACls with a basicity of 90%. One with a lower Ala percentage showed lower residual aluminum concentrations. Comparison of Figures A–B and C–D demonstrates superiority of Ala percentage over basicity as an index determining residual aluminum concentration, in particular for concentrations <0.1 mg/L. Residual aluminum concentrations <0.015 mg/L were attained by the PACls (Ala ≤0.5%, basicity ≥85%) even at a weakly alkaline pH of 8.0. The PACls exhibited residual aluminum concentrations <0.02 mg/L at a pH range of 6.5–8.5 (some data are shown Fig. 7). At the optimum pH at which residual aluminum concentration was minimized, residual aluminum concentrations were <0.007 mg/L. Residual aluminum concentrations after the coagulation by high-basicity PACls was studied previously (Yan et al., 2007; Yang et al., 2011). However, such low residual aluminum concentrations were not attained. Our study suggests that their non-attainment would be due to the high Ala percentage (>5%) even though the basicity was as high as 83%. In those studies, the observed residual aluminum concentration achieved with a PACl with 15.6% Ala was around 0.07–0.09 mg/L at pH 7.8 (Yang et al., 2011), and 0.1 mg/L with a PACl with 5.5% Ala at pH 8 (Yan et al., 2007). These data are roughly in line with our observation shown in Fig. 6. Notably, in our study the residual aluminum concentration drastically decreased to <0.015 mg/L at pH 8.0 when the Ala percentage of the PACl decreased to <0.5%.

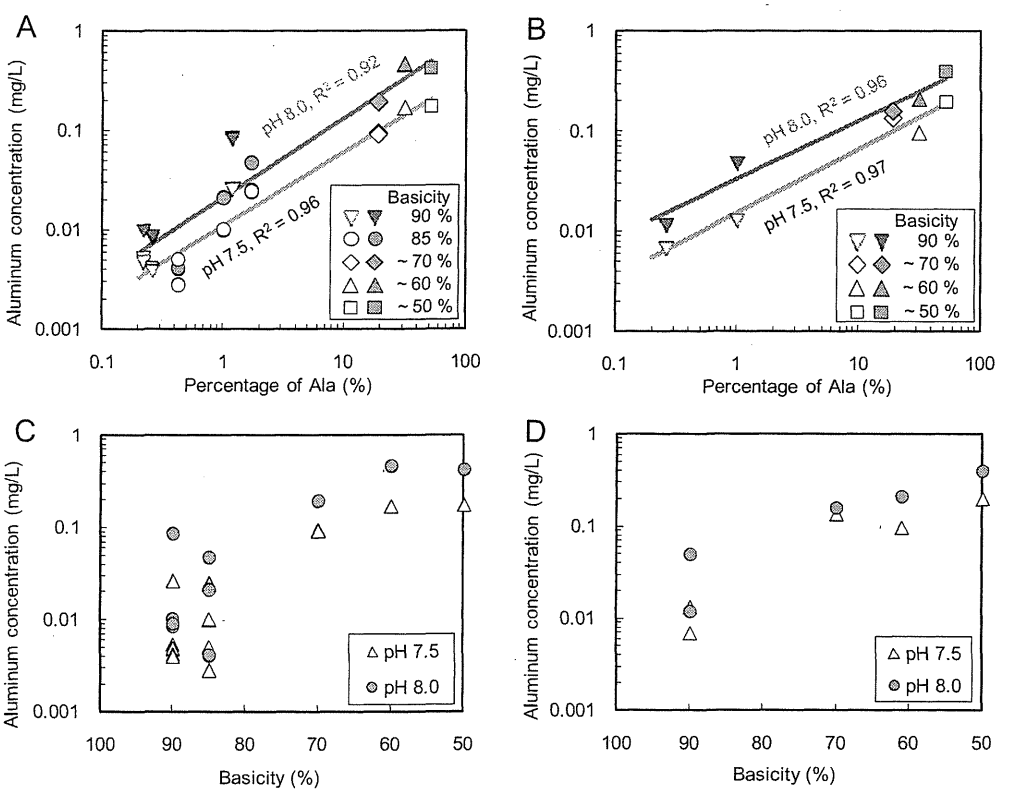

Fig. 6 – Effect of Ala percentage in PACls and their basicity on residual aluminum concentrations:(Panels A and C) Wani River water, coagulant dosage: 2.86 mg-Al/L; (Panels B and D)Toyohira River water C, coagulant dosage: 1.89 mg-Al/L.

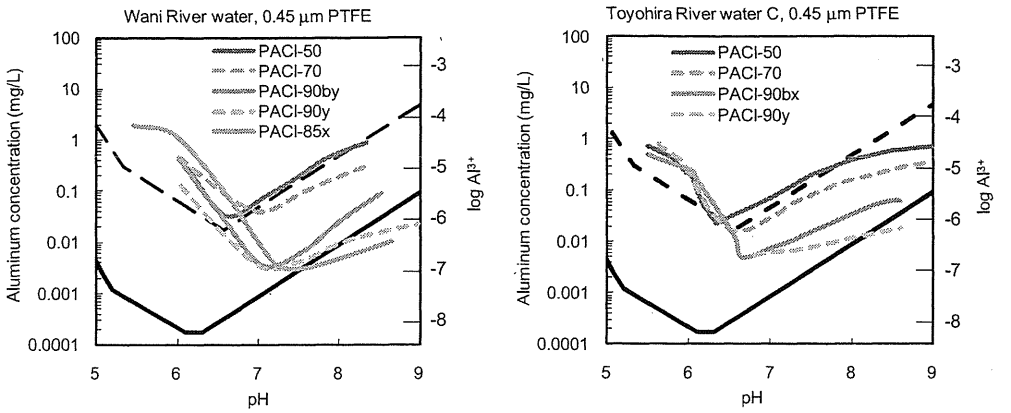

Fig. 7 – (solid black lines) Solubility diagram for aluminum at 20 °C calculated byGeochemist's Workbench, ver. 6 (RockWare, Inc., Golden, CO, USA), (dashed black lines) theoretical solubility for Al species in equilibrium with Al(OH)3(am) at 20 °C calculated by Pernitsky and Edzwald (2003), and experimentally observed residual aluminum concentrations of PACl-50, PACl-70, PACl-85x, PACl-90bx/90by, andPACl-90y (blue, red, pink, green, and light green lines, respectively). (For interpretation of the references to colour in this figure legend, the reader is referred to the web version of this article.)

In Fig. 7, experimentally observed residual aluminum concentrations were compared with the solubility of amorphous aluminum hydroxide and gibbsite ($AlOH_3$). For pH < 6.5, residual aluminum concentrations exceeded the solubility limit of amorphous $AlOH_3$. The residual aluminum concentrations for PACl-70 were below the solubility limit of amorphous $AlOH_3$ at pH > 7, but they exceeded the solubility limit of gibbsite. The residual aluminum concentrations of PACl-85x, PACl-90by, and PACl-90y were much lower than the amorphous aluminum solubility and closely approached the solubility limit of gibbsite. In particular, residual aluminum concentrations of PACl-85x and PACl-90y at pH > 7.5 were close to or lower than the aluminum solubility. These PACls are highly prehydrolyzed aluminum salts that are obtained by neutralizing the acidic polymer with base. In particular, the pH value of PACl-90y is 5.5, and the solubility diagrams (dashed and solid black lines) suggest the dissolved aluminum concentration at pH 5.5 is in agreement with the Ala content in PACl-90y (Fig. 1). Therefore, the low concentration of dissolved aluminum contained in this PACl would lead to a very low residual aluminum concentration after its dosing.

4. Conclusions

1. The amount of Ala in PACl mainly determined the dissolved residual aluminum concentration after coagulation, whereas polymeric (Alb)/colloidal (Alc) ratio in PACl did not affect dissolved residual aluminum concentration at a given basicity.
2. PACls with Ala ≤0.5% and basicity ≥85% yielded residual aluminum concentrations <0.007 mg/L at the optimum pH. Even at a wide pH range of 6.5–8.5 the concentration was always <0.02 mg/L. Residual aluminum concentrations at pH > 7.5 were close to or lower than the gibbsite solubility limit. The very low monomeric aluminum content inherent to these high-basicity PACls appears to have contributed to the very low residual aluminum concentration.
3. When coagulation was performed at pH > 6.5, dissolved residual aluminum concentration was reduced by using high-basicity PACls. For coagulation at pH < 6.5, the dissolved residual aluminum concentration was reduced by using sulfated PACls instead of non-sulfated PACls.
4. Dissolved residual aluminum was present in the fractions with MW ranges of 500 Da–3 kDa and 100 kDa–0.45 μm at pH 7.0, and aluminum was also present in the fraction with a MW range of 3–100 kDa at pH 7.5. The lower dissolved residual aluminum concentrations observed after treatment with PACl, compared with treatment with alum and $AlCl_3$, were due to the lower aluminum concentrations in the fractions at 100 kDa–0.45 μm. High-basicity PACls produced higher reductions in aluminum concentrations in the MW fractions at 500 Da–3 kDa, 3–100 kDa, and 100 kDa–0.45 μm.
5. The dissolved residual aluminum in the fraction with an MW range of 100 kDa–0.45 μm would have been dissolved aluminum–NOM complex formed from Ala (monomeric aluminum). The low dissolved residual aluminum concentrations observed after coagulation by high-basicity PACls may have been related partly to their low content of Ala, which tends to form dissolved aluminum–NOM complex.
6. Although increasing the dosage of normal-basicity PACls led to an increased dissolved residual aluminum concentration at pH 7.5, increasing the dosage of high-basicity PACls did not.
7. At higher raw water temperatures, the residual aluminum concentrations increased, yet the ability of high-basicity PACls to lower the residual aluminum concentration was maintained.

Acknowledgments

This study was supported by a Grant-in-Aid for Scientific Research S (24226012) from the Japan Society for the

Promotion of Science and by Health and Labour Sciences Research Grant (Research on Health Security Control) of Japan.

Appendix A. Supplementary data

Supplementary data related to this article can be found at http://dx.doi.org/10.1016/j.watres.2013.01.037.

REFERENCES

Amirtharaja, A., O'Melia, C.R., 1990. Coagulation processes: destabilization, mixing, and flocculation. In: Pontius, F.W. (Ed.), Water Quality & Treatment, fourth ed. McGraw-Hill.

Chen, Z., Fan, B., Peng, X., Zhang, Z., Fan, J., Luan, Z., 2006. Evaluation of Al_{30} polynuclear species in polyaluminum solutions as coagulant for water treatment. Chemosphere 64 (6), 912–918.

Chen, Z., Luan, Z., Fan, J., Zhang, Z., Peng, X., Fan, B., 2007. Effect of thermal treatment on the formation and transformation of Keggin Al13 and Al30 species in hydrolytic polymeric aluminum solutions. Colloids and Surfaces A: Physicochemical and Engineering Aspects 292 (2–3), 110–118.

Chen, Z., Luan, Z., Jia, Z., Li, X., 2009. Study on the hydrolysis/precipitation behavior of Keggin Al_{13} and Al_{30} polymers in polyaluminum solutions. Journal of Environmental Management 90 (8), 2831–2840.

Driscoll, C.T., Letterman, R.D., 1995. Factors regulating residual aluminium concentrations in treated waters. Environmetrics 6 (3), 287–309.

Flaten, T.P., 2001. Aluminium as a risk factor in Alzheimer's disease, with emphasis on drinking water. Brain Research Bulletin 55 (2), 187–196.

Gao, B.-Y., Chu, Y.-B., Yue, Q.-Y., Wang, B.-J., Wang.,, S.-G., 2005. Characterization and coagulation of a polyaluminum chloride (PAC) coagulant with high Al_{13} content. Journal of Environmental Management 76 (2), 143–147.

Gupta, V.B., Anitha, S., Hegde, M.L., Zecca, L., Garruto, R.M., Ravid, R., Shankar, S.K., Stein, R., Shanmugavelu, P., Jagannatha Rao, K.S., 2005. Aluminium in Alzheimer's disease: are we still at a crossroad? Cellular and Molecular Life Sciences 62 (2), 143–158.

Itoh, Y., Sato, K., 1995. Production of Sulfate-containing Basic Al Chloride. Japanese Patent, Application number 1993-181638, Publication number 1995-033432 (information available at: the web of Japan Patent Office, http://www.ipdl.inpit.go.jp/homepg_e.ipdl).

Jekel, M.R., Henizmann, B., 1989. Residual aluminum in drinking water treatment. Journal of Water Supply: Research & Technology AQUA 38, 281–288.

Jekel, M.R., 1991. Removal of aluminium in coagulation and acidic raw waters. Special Subject: aluminium in water: how can it be removed? Use of aluminium salts in treatment. In: Proc. IWSA (International Water Supply Association) 18th International Water Supply Conference and Exhibition. Copenhagen, Denmark, pp. SS8:1–SS8:4.

Jia, Z., He, F., Liu, Z., 2004. Synthesis of polyaluminum chloride with a membrane reactor: operating parameter effects and reaction pathways. Industrial & Engineering Chemistry Research 43 (1), 12–17.

Licsko, I., Szakal, F., 1988. Possibility of lowering the aluminium concentration in drinking water from water works drawing on surface water in Hungary. In: Astruc, M. (Ed.), Heavy Metal in the Hydrological Cycle. Selper Ltd, United Kingdom, pp. 631–636.

Lin, J.-L., Huang, C., Pan, J.R., Wang, D., 2008. Effect of Al(III) speciation on coagulation of highly turbid water. Chemosphere 72 (2), 189–196.

Miller, R.G., Kopfler, F.C., Kelty, K.C., Stober, J.A., Ulmer, N.S., 1984. The occurrence of aluminum in drinking water. Journal of the American Water Works Association 76 (1), 84–91.

Matsukawa, S., Itoho, S., Habuthu, S., Aizawa, T., 2006. An approach to residual aluminium control at Nisiya purification plant, Water Works Bureau, Yokohama. Water Science & Technology: Water Supply 6 (4), 67–74.

Ohno, K., Kadota, E., Matsui, Y., Kondo, Y., Matsushita, T., Magara, Y., 2009. Plant capacity affects some basic indices of treated water quality: multivariate statistical analysis of drinking water treatment plants in Japan. Journal of Water Supply: Research & Technology-AQUA 58 (7), 476–487.

Parthasarathya, N., Buffle, J., 1985. Study of polymeric aluminium(III) hydroxide solutions for application in waste water treatment. Properties of the polymer and optimal conditions of preparation. Water Research 19 (1), 25–36.

Pernitsky, D.J., Edzwald, J.K., 2003. Solubility of polyaluminium coagulants. Journal of Water Supply: Research & Technology-AQUA 52 (6), 395–406.

Sato, F., Matsuda, S., 2009. Novel Basic Aluminum Chloride, Its Manufacturing Method and Its Application. Japanese Patent, Application number 2008-047932, Publication number 2009-203125 (information available at: the web of Japan Patent Office, http://www.ipdl.inpit.go.jp/homepg_e.ipdl).

Shen, Y.-H., Dempsey, B.A., 1998. Synthesis and speciation of polyaluminum chloride for water treatment. Environment International 24 (8), 899–910.

Simpson, A.M., Hatton, W., Brokbank, M., 1988. Aluminum, its use and control, in potable water. Environmental Technology 9 (9), 907–916.

Van Benschoten, J.E., Edzwald, J.K., 1990. Measuring aluminum during water treatment: methodology and application. Journal of the American Water Works Association 82 (5), 71–78.

Van Benschoten, J.E., Jensen, J.N., Rahman, Md.A., 1994. Effects of temperature and pH on residual aluminum in alkaline waters. Journal of Environmental Engineering-ACSE 120 (3), 543–559.

Wang, D., Tang, H., Gregory, J., 2002. Relative importance of charge neutralization and precipitation on coagulation of kaolin with PACl: Effect of sulfate ion. Environmental Science & Technology 36 (8), 1815–1820.

Wang, W.-Z., Hsu, P.H., 1994. The nature of polynuclear OH-Al complexes in laboratory-hydrolyzed and commercial hydroxyaluminum solutions. Clays and Clay Minerals 42 (3), 356–368.

Wang, D., Suna, W., Xua, Y., Tang, H., Gregory, J., 2004. Speciation stability of inorganic polymer flocculant–PACl. Colloids and Surfaces A: Physicochemical and Engineering Aspects 243 (1–3), 1–10.

World Health Organization, 2004. Guidelines for Drinking – Water Quality. World Health Organization, Geneva, Switzerland, pp. 301–303.

Yan, M., Wang, D., Qu, J., He, W., Chow, C.W.K., 2007. Relative importance of hydrolyzed Al(III) species (Ala, Alb, and Alc) during coagulation with polyaluminum chloride: a case study with the typical micro-polluted source waters. Colloid and Interface Science 316 (2), 482–489.

Yan, M., Wang, D., Ni, J., Qu, J., Chow, C.W.K., Liu, H., 2008a. Mechanism of natural organic matter removal by polyaluminum chloride: effect of coagulant particle size and hydrolysis kinetics. Water Research 42 (13), 3361–3370.

Yan, M., Wang, D., Yu, J., Ni, J., Edwards, M., Qu, J., 2008b. Enhanced coagulation with polyaluminum chlorides: role of pH/Alkalinity and speciation. Chemosphere 71 (9), 1665–1673.

Yang, Z., Gao, B., Cao, B., Xu, W., Yue, Q., 2011. Effect of $OH^-/Al3^+$ ratio on the coagulation behavior and residual aluminum speciation of polyaluminum chloride (PAC) in surface water treatment. Separation and Purification Technology 80 (1), 59–66.

Regulatory Toxicology and Pharmacology 65 (2013) 108–114

Contents lists available at SciVerse ScienceDirect

Regulatory Toxicology and Pharmacology

journal homepage: www.elsevier.com/locate/yrtph

Safety assessment of boron by application of new uncertainty factors and their subdivision

Ryuichi Hasegawa [a], Mutsuko Hirata-Koizumi [a], Michael L. Dourson [b], Ann Parker [b], Atsushi Ono [a], Akihiko Hirose [a,*]

[a] National Institute of Health Sciences, 1-18-1 Kamiyoga, Setagaya-ku, Tokyo 158-8501, Japan
[b] Toxicology Excellence for Risk Assessment, 2300 Montana Avenue, Suite 409, Cincinnati, OH 45211, USA

ARTICLE INFO

Article history:
Received 12 June 2012
Available online 5 November 2012

Keywords:
Derivation of boron TDI
Chemical risk assessment
Application of new uncertainty factor (UF)
Subdivision of new uncertainty factor (UF)

ABSTRACT

The available toxicity information for boron was reevaluated and four appropriate toxicity studies were selected in order to derive a tolerable daily intake (TDI) using newly proposed uncertainty factors (UFs) presented in Hasegawa et al. (2010). No observed adverse effect levels (NOAELs) of 17.5 and 8.8 mg B/kg/day for the critical effect of testicular toxicity were found in 2-year rat and dog feeding studies. Also, the 95% lower confidence limit of the benchmark doses for 5% reduction of fetal body weight ($BMDL_{05}$) was calculated as 44.9 and 10.3 mg B/kg/day in mouse and rat developmental toxicity studies, respectively. Measured values available for differences in boron clearance between rats and humans and variability in the glomerular filtration rate (GFR) in pregnant women were used to derive chemical specific UFs. For the remaining uncertainty, newly proposed default UFs, which were derived from the latest applicable information with a probabilistic approach, and their subdivided factors for toxicokinetic and toxicodynamic variability were applied. Finally, overall UFs were calculated as 68 for rat testicular toxicity, 40 for dog testicular toxicity, 247 for mouse developmental toxicity and 78 for rat developmental toxicity. It is concluded that 0.13 mg B/kg/day is the most appropriate TDI for boron, based on rat developmental toxicity.

1. Introduction

To ensure drinking water safety, a variety of toxicity information on environmental pollutant chemicals is collected and evaluated in order to derive a tolerable daily intake (TDI). A TDI is derived by dividing the no observed adverse effect level (NOAEL) for the selected critical effect (identified from key toxicity studies such as repeated dose toxicity, reproductive and developmental toxicity, and carcinogenicity) by an appropriate composite uncertainty factor (UF). A default composite UF of 100, consisting of 10 for interspecies differences (UF_a) and 10 for human variability (UF_h), has been commonly used in the derivation of TDIs in Japan and some international organizations. WHO (2005) took the approach further by determining that each component UF can be subdivided into toxicokinetics (TK), disposition of substance (generally measured as species differences in blood concentration at the same dose), and toxicodynamics (TD), toxic intensity of substances (generally measured as species differences in toxicity level at the same blood concentration). Appropriate measured or estimated TK and/or TD values can be incorporated into the safety assessment process by replacing the default component UFs.

To date, this subdivision approach has been applied in several situations in Health Canada (Meek et al., 1994) and the United States (US EPA, 2004), but the approach is limited internationally. The WHO drinking water quality guidelines used the approach for boron, where measured data on the human glomerular filtration rate (GFR) was used to determine the chemical specific UF used in the TDI calculation (WHO, 2009). However, an even newer approach for UF selection has been derived from the latest data related to interspecies differences and human variability with a probabilistic approach to the TK and TD subdivisions (Hasegawa et al., 2010). Therefore, in this article, we apply the new UF probabilistic subdivisions during the UF selection process in order to derive a TDI for boron.

2. Concept of current uncertainty factor

An UF of 100 (Lehman and Fitzhugh, 1954) was proposed for boron without substantial reasons, as was common practice, and has been widely used around the world until recently. Dourson and Stara (1983) justified using an UF of 100 ($UF_a = 10$, $UF_h = 10$) in risk calculations by gathering and organizing supporting

* Corresponding author. Address: Division of Risk Assessment, Biological Safety Research Center, National Institute of Health Sciences, 1-18-1 Kamiyoga, Setagaya-ku, Tokyo 158-8501, Japan. Fax: +81 3 3700 1408.
E-mail address: hirose@nihs.go.jp (A. Hirose).

0273-2300/$ - see front matter © 2012 Elsevier Inc. All rights reserved.
http://dx.doi.org/10.1016/j.yrtph.2012.10.013

information. Analysis of interspecies differences (Freireich et al., 1966) demonstrated a good relationship between the body surface area and the maximum tolerated dose of 18 anti-cancer drugs after repeated administration in humans and various experimental animals. The body surface area can be presented as:

$$BW^{2/3} \times K \times 10^{-4}\ m^2$$

the body surface area per body weight becomes:

$$BW^{2/3} \times K \times 10^{-4} \times BW^{-1} = K \times 10^{-4} \times BW^{-1/3}$$

where BW is the body weight (g) and K is an adjustment factor.

As K ranges from 9 to 11 in various experimental animals as well as humans, the body surface ratio of animal/human is:

$$K_a \times 10^{-4} \times BW_a^{-1/3} / K_h \times 10^{-4} \times BW_h^{-1/3} = BW_h^{1/3}/BW_a^{1/3} = (BW_h/BW_a)^{1/3}.$$

The body surface correction factor becomes 5.6 for rats and 11.4 for mice when the body weight is 60 kg for humans, 350 g for rats and 40 g for mice. Based on these data, a default UF_a of 10 is considered to be an appropriate numerical value, since it lies between these two values. When logarithmic dose/probit slopes were calculated for acute rat toxicity data on 490 chemicals, 92% of the slopes were 3 or greater, suggesting that a 10-fold decrease in dose would yield a 3 probit reduction in risk. This supports the use of an UF_h of 10 for within species variability.

Renwick (1993) proposed that the UF_a and UF_h can each be subdivided into a TK and TD component. Renwick analyzed toxicokinetic parameter data, such as clearance rate and area under the concentration time curve (AUC) in plasma or tissue for TK and *in vitro* dose–response or *in vivo* toxicodynamic data were analyzed for TD to support the UF division. IPCS and WHO (IPCS, 1994; WHO, 2005) determined that the distribution of the TK:TD ratio is 60:40 for UF_a and 50:50 for UF_h:

$$UF_a = (TK) \times (TD) = 10^{0.6} \times 10^{0.4} = 4\ (TK) \times 2.5\ (TD)$$

$$UF_h = (TK) \times (TD) = 10^{0.5} \times 10^{0.5} = 3.2\ (TK) \times 3.2\ (TD).$$

The default value of 4 for UF_a (TK) is consistent with the differences in fundamental physiological parameters, for example, the heart output volume of rats is approximately 4-fold higher than in humans. The equal subdivision of UF_h is supported by the analysis of kinetic parameters for 60 chemicals and toxicity dose–response data for 49 chemicals.

3. Toxicity-related information on boron

Boron has almost complete absorption via the gastrointestinal tract and is excreted via the urine in both humans and experimental animals. The average clearance rate for boron is 163 mL/h/kg (2.72 mL/min/kg) in rats and 41 mL/h/kg (0.68 mL/min/kg) in humans, the rat clearance value is approximately 4-fold higher than the human value (Dourson et al., 1998). Boron clearance in pregnant women averages at 1.02 mL/min/kg (66.1 mL/min/person) (Pahl et al., 2001) and the rate in pregnant rats is 3.3 mL/min/kg (1.0 mL/min/rat) (Vaziri et al., 2001), indicating that boron clearance rates increase during pregnancy by 50% in humans and 21% in rats.

Evidence of human male reproductive toxicity was not observed in the epidemiological studies of men exposed to high levels of boron (Sayli, 2001, 2003; Whorton et al., 1994; Yazbeck et al., 2005; Robbins et al., 2010; Duydu et al., 2011). However, testicular and developmental toxicity were observed in multiple experimental animal toxicity studies. Boron was neither genotoxic nor carcinogenic in cancer bioassays (NTP, 1987).

Nine repeat dose toxicity studies and five reproductive/developmental toxicity studies for boric acid were evaluated in order to derive a TDI for boron. Brief study details and NOAELs for selected target organs or endpoints are shown in Table 1. NOAELs are expressed as mg B (boron)/kg (body weight)/day, which are converted to mg of boron by multiplying by the ratio of the molecular weight of boron to the molecular weight of boric acid (10.81/61.84 = 0.1748).

4. Derivation of boron TDI in WHO and US

4.1. Drinking water quality guideline in WHO (2009)

The critical endpoint of interest for boron was determined to be fetal body weight changes and skeleton malformations (high incidence of short rib XIII and wavy ribs) observed in two rat developmental toxicity studies (Heindel et al., 1992; Price et al., 1996b). The 95% lower confidence limit of the benchmark dose for 5% reduction of fetal body weight ($BMDL_{05}$ = 10.3 mg B/kg/day) (Allen et al., 1996) was adopted as the point of departure (POD) for this evaluation.

The available boron data was not sufficient to derive a chemical specific interspecies UF, thus the default UF of 10 was used. The UF for human variability was subdivided into TK and TD components according to the WHO methodology (IPCS, 1994; WHO, 2005). TK data from pregnant women were analyzed as a sensitive subpopulation to determine the TK portion of the UF_h. Given that boron is essentially not metabolized and is mostly excreted via the urine, the GFR in pregnant women is used in place of the default TK UF_h. Dourson et al. (1998) combined data from multiple studies obtaining a GFR of 144 ± 32 mL/min for healthy pregnant women in their last trimester. In order to account for 95% of the population, the average GFR_A (144 mL/min) was divided by the GFR_{2SD} at two standard deviations below the average ($GFR_A - GFR_{2SD}$ = 144 − 2 × 32 = 80 mL/min), resulting in a human TK variability UF_h of 1.8 (144/80 = 1.8) (Dourson et al., 1998). There were no data on TD variation in pregnant women, therefore the default TD UF_h of 3.2 was used. The resulting human variability UF is approximately 6; derived by multiplying the TK and TD values together (1.8 × 3.2 = 5.7).

Finally, a TDI of 0.20 mg B/kg/day was derived by applying the composite UF of 60 ($UF_a \times UF_h = 10 \times 6$) to the $BMDL_{05}$ of 10.3 mg B/kg/day for rat developmental toxicity.

$$\frac{10.3\ \text{mg B/kg/day}}{60} = 0.2\ \text{mg B/kg/day}$$

4.2. Toxicological review by US EPA (2004)

As with WHO, combined data on fetal body weight changes, rib XIII effects and variations of the first lumbar rib from two rat developmental toxicity studies (Heindel et al., 1992; Price et al., 1996b) were selected as the critical endpoints, and the $BMDL_{05}$ of 10.3 mg B/kg/day calculated for reduction of fetal body weight by Allen et al. (1996) was selected as the POD.

In a slightly different approach US EPA subdivided the default UF of 10 for UF_a and UF_h into 3.16 for TK variability and 3.16 for TD variability in animals and humans. As there was no TD data for interspecies differences and human variability, only TK data were analyzed. TK analysis was conducted for differences between pregnant rats and women (species difference) and for variations in pregnant women (human variability). Boron is easily absorbed after oral administration in both humans and animals, but is not metabolized in the body. More than 90% of the absorbed boron was excreted in a short period via the urine. In humans, 92–94%

Table 1
Summary of repeat dose, developmental toxicity, and generation studies for boric acid.

Species	Route	Period	Target	NOAEL[a]	References
Repeated dose toxicity study					
Rats	Feeding	28 d	Testes	61[b]	Treinen and Chapin (1991)
Rats	Feeding	30–60 d	Testes	25	Lee et al. (1978)
Rats	Feeding	9 w	Testes	26[b]	Ku et al. (1991)
Mice	Feeding	13 w	Testes	70	Dieter (1994)
Rats	Feeding	90 d	Testes	38	Weir and Fisher (1972)
Dogs	Feeding	90 d	Testes	3.9	Weir and Fisher (1972)
Mice	Feeding	2 y	Testes	48	Dieter (1994)
Rats	Feeding	2 y	Testes	17.5	Weir and Fisher (1972)
Dogs	Feeding	2 y	Testes	8.8	Weir and Fisher (1972)
Developmental or generation toxicity study					
Mice	Feeding	gd 0–17	Fetal bw	43	Heindel et al. (1992)
Rats	Feeding	gd 0–20	Fetal bw	14[b]	Heindel et al. (1992)
Rats	Feeding	gd 0–20	Fetal tox	9.6	Price et al. (1996b)
Rats	Feeding	3 gen	Reproduction	17.5	Weir and Fisher (1972)
Rabbits	Gavage	gd 6–19	Fetal tox	22	Price et al. (1996a)

d: Day; w: week; y: year; gd: gestational day; bw: body weight; gen: generation; tox: toxicity.
[a] mg B/kg/day.
[b] Lowest observed adverse effect level.

of boron was excreted as the unchanged form in urine after 96 h of digestion. In rats, boron was completely absorbed within 24 h, the absorbed boron was uniformly distributed throughout the body and the 95% was excreted in urine over 3 days. Thus, it is considered that the disposition of boron is the same in humans and animals.

To assess interspecies TK differences, UF_a (TK), boron clearance was compared between pregnant rats and pregnant women. The study assessed on pregnant rats given 0.3, 3.0 or 30 mg B/kg orally showed the dose-independent value of boron clearance as 1.00 mL/min (Vaziri et al., 2001; US Borax, 2000). For human assessment, after 15 pregnant women had eaten fruits and vegetables containing a high content of boron, the concentration of boron in blood and urine was determined for the first two hours, resulting in a 66.1 mL/min boron clearance (Pahl et al., 2001; US Borax, 2000). The steady state blood concentration (Css) of boron in the 2-compartment model can be expressed as follows:

$$Css = \frac{Dose \times f \times BW}{Cl}$$

where f is the absorption rate, BW is body weight, and Cl is clearance. When pregnant rats and women have equal blood concentrations of boron, differences in the administered dose can be adopted as the UF_a (TK). Therefore, using the boron absorption rate of humans (f_h) – 0.92 (Schou et al., 1984), the rate of rats (f_a) – 0.95 (Vanderpool et al., 1994), the body weight of pregnant women – 67.6 kg (Pahl et al., 2001) and that of pregnant rats – 0.303 kg (Vaziri et al., 2001), the UF_a (TK) was calculated as follows:

$$\frac{Dose_a}{Dose_h} = UF_a(TK) = \frac{Cl_a \times f_h \times BW_h}{Cl_h \times f_a \times BW_a} = \frac{1.00 \times 0.92 \times 67.6}{66.1 \times 0.95 \times 0.303} = \frac{62.192}{19.027} = 3.3$$

An UF_a of 10.4 results from $TK_a \times TD_a$ (3.3 × 3.16).

Adoption of boron clearance data of pregnant women used for the interspecies TK differences (Pahl et al., 2001) was considered for the human variability UF. However, US EPA determined that the Pahl et al. (2001) study could not be used because the number of subjects was inadequate and the boron content of the food was not controlled. Therefore, GFR data from healthy pregnant women (Dunlop, 1981; Krutzen et al., 1992; Sturgiss et al., 1996) were used as a surrogate for boron clearance. In order to account for pregnant women with very low GFR, particularly when preeclampsia is present, the average GFR_A was divided by the GFR_{3SD} at three standard deviations below the average (GFR_A–GFR_{3SD}) to calculate UF_h (TK) (Dourson et al., 1998) (Table 2). An UF_h of 6.3 results from $TK_h \times TD_h$ (2.0 × 3.16).

Finally, an oral RfD of 0.20 mg B/kg/day was derived by applying the composite UF of 66 (3.3 × 3.16 × 2.0 × 3.16) to the $BMDL_{05}$ of 10.3 mg B/kg/day for rat developmental toxicity.

$$\frac{10.3 \text{ mg B/kg/day}}{66} = 0.2 \text{ mg B/kg/day}$$

5. Concept of new uncertainty factors

Recently, the metabolic rate or caloric demand correction was demonstrated to be more appropriate than body surface correction when determining interspecies differences for UFs (Schneider et al., 2004). Body surface area is proportional to 2/3 power of body weight, while metabolic rate or caloric demand is proportional to 3/4 power of body weight.

$$\text{Caloric demand} = f \times BW^{3/4}$$

$$\text{Caloric demand/body weight} = f \times BW^{3/4} \times BW^{-1} = f \times BW^{-1/4}$$

Then, the animal/human ratio for metabolic rate or caloric demand per body weight is:

$$\frac{\text{Caloric demand of animal/body weight}}{\text{Caloric demand of human/body weight}} = \frac{f_a \times BW_a^{-1/4}}{f_h \times BW_h^{-1/4}} = \frac{BW_h^{1/4}}{BW_a^{1/4}} = \left(\frac{BW_h}{BW_a}\right)^{1/4}$$

Table 2
Variation of glomerular filtration rate in healthy pregnant women.

$GFR_A \pm SD$ (mL/min)	GFR_A–GFR_{3SD}	UF_h (TK)	References
150.5 ± 17.6[a]	97.7	1.54	Dunlop (1981)
195 ± 32[b]	99	1.97	Krutzen et al. (1992)
138.9 ± 26.1[c]	60.6	2.29	Sturgiss et al. (1996)
	Average of above data	1.93	

[a] Combined data of individual average of GFRs at 12, 26 and 36 weeks of pregnancy in 25 healthy women.
[b] Combined data of 13 healthy pregnant women in the last trimester.
[c] Combined data of individual average of GFRs in early and late pregnancy in 21 healthy women.

where f is the absorption rate and BW is body weight. When the body weights of humans, rats and mice are 60 kg, 350 g and 40 g, respectively, the caloric demand correction factor is 3.6 for rats and 6.2 for mice, which are less than the default UF_a of 10. However, it should be noted that these correction values are derived using median values for animals and humans, thus do not sufficiently cover the possible range of variation. Schneider et al. (2004) compared human and various experimental animal maximum tolerated dose data for 63 anti-cancer drugs, this analysis demonstrates the appropriateness of using the geometric standard deviation along with caloric demand correction values as medians to cover 95% of the variation. When the 95th percentile of caloric demand correction is calculated for animals to humans, the correction is 38 for mice and 27 for rats, indicating that an UF_a of 10 is not sufficient. Falk-Filipsson et al. (2007) agreed with the appropriateness of this caloric demand correction for interspecies differences.

The difference between NOAELs in the standard human population and the sensitive subpopulation are considered the most appropriate data for determining human variability. However, this type of human data is limited, generally making the use of experimental animal data inevitable. Among sensitive subpopulations, the effects on pregnant women and the elderly are evaluated by reproductive/developmental and chronic toxicity studies, respectively. Newborn animals are another sensitive subpopulation but toxicity studies are not usually conducted for them because there are no officially agreed upon testing guidelines. Recently, a comparative analysis of NOAELs in newborn and young rats from repeated dose toxicity studies of 18 chemicals was conducted (Hasegawa et al., 2007). As a result, the median ratio for the NOAELs (young/newborn rats) was 3 with a geometric standard deviation of 1.38 (Hasegawa et al., 2010).

Based on these considerations, new UFs for each animal, which were calculated by multiplying two log-normal distribution data for interspecies differences and human variability with a probabilistic approach, were proposed as shown in Table 3 (Hasegawa et al., 2010).

Based on the information found in Table 3, new subdivision default values for each animal were proposed, as shown in Table 4. Consistent with the information found in Table 3, the contribution ratio of interspecies differences depends on animal size. For example, the new proposed UF of 100 for hamsters and rats approximates either 111 or 88.7. Using the contribution ratio, the default 100 factor can be subdivided as either 25 and 4 for UF_a and UF_h, respectively. Furthermore, for subdivision of the default UF_a and UF_h, the ratio distribution used by WHO was applied, 60:40 for TK and TD for interspecies differences (UF_a) and 50:50 for TK and TD for human variability (UF_h). As a result, the default UF_a of 25 is subdivided into 7.0 (TK) and 3.6 (TD), and the default UF_h of 4.0 is subdivided into 2.0 for both TK and TD. When appropriate measured data or PBPK data are available, that data can be used instead of the subdivision default values; otherwise, the given default subdivision values should be used.

Table 3
Proposal of new uncertainty factors for each animal.

Species	UF_a	UF_h	$UF_a \times UF_h$	Proposal
Mice	48.2	5.09	155	150
Hamsters	34.4	5.09	111	100
Rats	27.5	5.09	88.7	
Rabbits	13.8	5.09	44.3	40
Monkeys	11.7	5.09	37.7	
Dogs	9.63	5.09	31.0	

UF_a: 95th percentile of interspecies differences between each animal and human based on caloric demand correction and geometric standard deviation of 3.23.
UF_h: 95th percentile of human variability based on median of 3.0 and geometric standard deviation of 1.38.

Table 4
Proposal of subdivision default for new uncertainty factors.

Species	Proposal of New UF	Default UF_a Default UF_h	Subdivision default TK × TD
Mice	150	UF_a: 38 UF_h: 4.0	9.0 × 4.3 2.0 × 2.0
Hamsters Rats	100	UF_a: 25 UF_h: 4.0	7.0 × 3.6 2.0 × 2.0
Rabbits Monkeys Dogs	40	UF_a: 10 UF_h: 4.0	4.0 × 2.5 2.0 × 2.0

6. Application of new uncertainty factors and their subdivision

We reviewed the available data for critical endpoints to calculate a TDI using the proposed new UFs with the subdivision default values described in Table 4. From the 14 toxicity endpoints shown in Table 1, two repeat dose studies and two developmental studies were selected as the appropriate data sets to derive a TDI. For each endpoint, the NOAEL/BMDL is obtained, followed by application of newly proposed UFs with subdivisions in order to derive a TDI.

In a 2-year rat feeding study (Weir and Fisher, 1972), testicular toxicity was found at 1170 ppm (58.5 mg B/kg/day), with 350 ppm (17.5 mg B/kg/day) as the NOAEL. Since toxicity was found only at the highest dose of 1170 ppm, application of the BMD approach was not appropriate.

The UF assessment for the testicular toxicity endpoint in male rats, UF_a (TK), was estimated on the basis of boron clearance in male rats and adult men. Boron clearance in male rats reported by Usuda et al. (1998) was 0.359 mL/min/100 g BW and in male volunteers reported by Jansen et al. (1984) was 54.6 mL/min/1.73m^2 (equivalent to 72 kg body weight). Using the US EPA UF formula the UF_a (TK) becomes 4.6 as follows:

$$\frac{\text{Dose}_a}{\text{Dose}_h} = \text{UF}_a(\text{TK}) = \frac{\text{Cl}_a \times f_h \times \text{BW}_h}{\text{Cl}_h \times f_a \times \text{BW}_a} = \frac{0.359 \times 0.92 \times 72}{54.6 \times 0.95 \times 0.10} = \frac{24}{5.2} = 4.6$$

where f is the absorption rate, BW is body weight, and Cl is clearance. TD data is lacking, therefore, the UF_a is 17 resulting from 4.6 × 3.6, the latter value from Table 4.

UF_h is generally the difference in NOAELs between the standard human population and the sensitive subpopulation. Male children should especially be considered as an appropriate target population because they are usually sensitive to the endpoint of interest (testicular toxicity). However, information on boron clearance or GFR in male children is not available. Furthermore, no reports of testicular abnormalities were found for fetuses exposed in utero, pups exposed in multiple generation studies, or male children exposed to boron. Therefore, a default factor of 4.0 for UF_h from Table 4 was applied.

By applying a UF of 70, resulting from $UF_a \times UF_h = 17 \times 4.0 = 68$ (rounded to 70), the TDI becomes 0.26 mg B/kg/day, based on a NOAEL of 17.5 mg B/kg/day for testicular toxicity in rats.

In a 2-year dog feeding study (Weir and Fisher, 1972), no toxic effects were observed at the highest dose of 350 ppm (8.8 mg B/kg/day), reported as the NOAEL. In a 90-day dog feeding study, testicular toxicity clearly appeared at 1750 ppm (30.4 mg B/kg/day) and toxicity at 1,170 ppm (29 mg B/kg/day) was also observed in a 26-week dog feeding study (Weir and Fisher, 1972). Therefore, it is deduced that testicular toxicity in dogs seems to not develop further in association with longer exposure.

No data are available on interspecies TK and TD differences for testicular toxicity in male dogs. As there are also no available data on human variability, as mentioned above, the integrated default UF of 40 from Table 4 was used. In the targeted dog study, the exposure period was 2 years, not lifetime exposure; however, an additional UF was not considered necessary because testicular toxicity appearing after 90-day exposure was not enhanced by significantly longer exposure (i.e. 26 weeks). Therefore, a TDI based on testicular toxicity in dogs is 0.22 mg B/kg/day, resulting from dividing the NOAEL of 8.8 mg B/kg/day by the UF of 40.

The incidence of malformation (especially shortening of rib XIII) was increased in mice given a diet containing 0.4% boric acid on gestation days 0–17 (Heindel et al., 1992); fetal body weight was also decreased at dietary concentrations of more than 0.2%. The NOAEL was 0.1% (43 mg B/kg/day) based on reduced fetal body weight. The BMD approach resulted in 44.9 mg B/kg/day of $BMDL_{05}$ for fetal body weight reduction.

For the assessment of developmental toxicity in mice, the default UF_a of 38 was applied to the $BMDL_{05}$, as there are no available data on interspecies differences.

The UF_h (TK) was evaluated by reviewing boron clearance variation data in pregnant women (Pahl et al., 2001). However, this data was judged to be inappropriate because the available study was not designed to evaluate human variability (low number of subjects and uncontrolled dietary intake of boron). Therefore, three GFR data in healthy pregnant women used by EPA and additional GFR data in pregnant subjects suffering from hypertension, preeclampsia and diabetes reported by Krutzen et al. (1992) (Table 5) were examined in order to evaluate human TK. In contrast to the US EPA approach, the difference between the average value in the standard population and the lower 95th percentile GFR in the sensitive subpopulation was considered to be more appropriate for human variability. In this case, average GFR in healthy pregnant women was used as the average in the standard population and the two Standard deviation below the average (GFR_A–GFR_{2SD}) in pregnant subjects suffering from preeclampsia, who have the lowest GFR among diseased pregnant subjects, was used as the value for the most sensitive pregnant subjects. Since the three GFR measurements in healthy pregnant women were quite different from each other, the one reported by Krutzen et al. (1992) was selected because the GFR appears to have been obtained according to the same protocol as GFR of preeclampsia subjects. Therefore, an UF_h (TK) of 3.23 from 195/60.3 was determined and the UF_h of 6.5 was developed by multiplying by the default UF_h (TD) of 2.0 due to lack of available data.

Therefore, the overall UF is 247 calculated from 38 × 6.5. TDI based on mouse developmental toxicity was 0.18 mg B/kg/day calculated by dividing the $BMDL_{05}$ of 44.9 mg B/kg/day by the UF of 247.

In a rat developmental study, boric acid was given via the diet on gestation days 0–20, and reduction of body weight and skeleton malformation of the fetus were observed at dietary concentrations of more than 0.1% (12.9 mg B/kg/day) (Heindel et al., 1992). The same study protocol was used for a lower dose range from 0.025%, resulting in a good dose–response outcome (Price et al., 1996b). Allen et al. (1996) analyzed the combined data from these two studies using the BMD approach, resulting in a $BMDL_{05}$ of 10.3 mg B/kg/day for reduced fetal body weight.

In order to assess the developmental toxicity in rats, boron clearance data were obtained for pregnant rats (Vaziri et al., 2001) and pregnant women (Pahl et al., 2001). Based on these data, the UF_a (TK) was 3.3 using the same US EPA method, as shown above. Due to the lack of available interspecies TD data, the UF_a is 12, calculated from 3.3 (default) × 3.6.

The UF_h (TK) of 3.23 was derived from average the GFR in healthy pregnant women and the lower 95th percentile GFR in preeclampsia pregnant subjects reported by Krutzen et al. (1992), as shown above. Due to the lack of available data for UF_h (TD), the UF_h is 6.5, calculated by 3.23 × 2.

Accordingly, by applying an UF of 78, resulting from UF_a - × UF_h = 12 × 6.5 = 78, to the $BMDL_{05}$ of 10.3 mg B/kg/day, the TDI based on rat developmental toxicity was 0.13 mg B/kg/day.

The four resultant TDI calculations are summarized in Table 6. The lowest TDI is obtained from the $BMDL_{05}$ of 10.3 mg B/kg/day in the rat developmental study, by applying the evidence-based UF_a(TK) and UF_h(TK) with the default TDs.

Table 5
Glomerular filtration rate in healthy and diseased pregnant subjects.

Subjects	No.	$GFR_A \pm SD$ (mL/min)	GFR_A–GFR_{2SD}
Healthy[a]	25	150.5 ± 17.6	115.3
Healthy[b]	21	138.9 ± 26.1	86.7
Healthy[c]	13	195 ± 32	131
Hypertension[c]	8	198.9 ± 57.9	83.1
Preeclampsia[c]	12	128.1 ± 33.9	60.3
Diabetic[c]	20	169 ± 34.7	99.6

[a] Dunlop (1981).
[b] Sturgiss et al. (1996).
[c] Krutzen et al. (1992).

7. Discussion and conclusion

A default UF of 10 for interspecies differences has commonly been used for all experimental animals even though there are marked size differences (e.g., approximately 500-fold from mice to dogs). For over 20 years, US EPA and ICH (Connelly et al., 1997) have used body surface correction, but it has been suggested that the metabolic rate or caloric demand correction may be more

Table 6
TDI derivation trial using available TK data.

Toxicity endpoints NOAEL/$BMDL_{05}$	Subdivision of UF_a	Subdivision of UF_h	TDI
Rats: testes NOAEL = 17.5 mg B/kg/day	TK = 4.58 TD = 3.6 (default) →**17**	UF_h = 4.0 (default)	UF = 68 0.26 mg B/kg/day
Dogs: testes NOAEL = 8.8 mg B/kg/day	UF_a = 10 (default)	UF_h = 4.0 (default)	UF = 40 (default) 0.22 mg B/kg/day
Mice: development $BMDL_{05}$ = 44.9 mg B/kg/day	UF_a = 38 (default)	TK = 3.23 TD = 2.0 (default) →6.5	UF = 247 0.18 mg B/kg/day
Rats: development $BMDL_{05}$ = 10.3 mg B/kg/day	TK = 3.3 TD = 3.6 (default) →12	TK = 3.23 TD = 2.0 (default) →6.5	UF = 78 0.13 mg B/kg/day

appropriate (Schneider et al., 2004; Falk-Filipsson et al., 2007). Recently, an integrated UF method has been proposed, incorporating new information on human variability (Hasegawa et al., 2010). However, TK and TD subdivision have only been applied for cases of boron in the drinking water quality guidelines in WHO (WHO, 2009) and US EPA (US EPA, 2004). The subdivision has been not applied in Japan, even though the application potential has been discussed. In this article, under these circumstances, we apply the new UFs and subdivisions for the safety assessment of boron.

Borate or borax is easily absorbed via the gastrointestinal tract and excreted in both humans and experimental animals. Borax becomes boric acid during absorption, boric acid is neither metabolized nor accumulated in the body and is excreted relatively quickly by the kidney; therefore, boron clearance is considered to approximate the boron blood concentration. Boron clearance in humans and rats, calculated from the boron blood concentration and excretion in urine for a certain period after oral administration of boric acid, was the TK data used for the UF_a. Boron clearance studies in rats, two reports in adult males (Usuda et al., 1998) and non-pregnant and pregnant females (Vaziri et al., 2001) were used to determine the clearance rate. There are two human studies of adult men (Jansen et al., 1984) and non-pregnant and pregnant women (Pahl et al., 2001). The former human study was reported from Denmark and the latter from the USA. There is no mention of race, but likely they were people of western decent. As there are no reports on boron clearance in Japan, it is necessary to consider whether the above human data can apply to people of East Asian decent including Japanese. Comparing the above two human data, there were no sex differences in boron clearance: 54.6 ± 8.0 mL/min/1.73m^2 in adult men versus 54.31 ± 19.35 mL/min/1.73m^2 in nonpregnant women. In pregnancy, clearance increased by approximately 25% (68.30 ± 35.00 mL/min/1.73m^2). Pahl et al. (2001) determined creatinine clearance (123.0 ± 23.8 mL/min/1.73m^2) along with boron clearance in non-pregnant women, which is about double that of boron clearance, the difference indicating that boron is reabsorbed by human renal tubular cells. In Japan, the normal creatinine clearance range is 70–130 mL/min, and abnormal values ranging from 50 to 70 mL/min, 30 to 50 mL/min, and <30 mL/min; these values suggest slight, moderate and severe kidney damage, respectively. Creatinine clearance is expressed as mL/min in Japan, but this actually means mL/min/1.73m^2. Therefore, Japanese creatinine clearance is considered to be almost equal to that in the western people, and boron clearance data obtained from western people is considered able to be directly applied to Japanese.

As for UF_a (TK), appropriate boron clearance data for rats and humans were obtained and the calculation formula given by (US EPA, 2004) was applied. On the other hand, to consider TK variability in pregnant women, WHO and US EPA adopted GFR variation data in healthy pregnant women to adequately cover pregnant women with very low GFR. WHO used UF_h (TK) of 1.8 on the basis of $GFR_A/(GFR_A-GFR_{2SD})$ from the data of late pregnant women in three reports (Dunlop, 1981; Krutzen et al., 1992; Sturgiss et al., 1996), and US EPA used UF_h (TK) of 2.0 given as an average of three values; $GFR_A/(GFR_A-GFR_{3SD})$ for early to late pregnant women in the same three reports. However, we understand that human variability means how much the values differ between the standard population and sensitive subpopulation. In this case, it should be considered that a standard population is healthy pregnant women and a sensitive subpopulation is pregnant subjects suffering from the most concerned disease, preeclampsia. There is only one report on preeclampsia, which clearly indicates lower GFR than in other pregnant women. We therefore decided to use the lower 95th percentile GFR in preeclampsia subjects and average GFR in healthy pregnant women in the same report (Krutzen et al., 1992). These data and the UF_h (TK) calculation method are considered to be preferable from the aspect of sufficient safety.

Other groups have developed tolerable upper intake limits, which are similar to the TDIs described here. For example, an Upper Limit (UL) for boron was developed by the US Institute of Medicine (US IOM, 2001) based on the same animal study but using a NOAEL for the same endpoint rather than BMDL. The NOAEL of 9.6 mg B/kg/day was divided by an UF of 30, resulting in an UL of 0.3 mg B/kg/day. For interspecies differences, the usual default value of 10 was selected but an UF of 3 was chosen for intraspecies variability, in view of the expected similarity in toxicokinetics among humans, leading to yield a UF of 30. Subsequently, the European Food Safety Authority (2004) developed an UL based on the same NOAEL of 9.6 mg B/kg/day but divided by an UF of 60 to allow for variability between rats and humans and between-person variability in humans. The resulting UL was 0.16 mg B/kg/day (EFSA, 2004). In a review of information developed for the Pesticide Management Regulatory Authority (PMRA) of Health Canada by an independent scientific panel, it was concluded that a BMDL of 14 mg B/kg/day could be developed from testicular effects in dogs and that a combined UF of approximately 160 would be appropriate. This UF consisted of a 3-fold factor for database concerns, a 6.4 factor for intraspecies variability, and a 8.3 factor for interspecies variability (Chapin et al., Submitted for publication).

This article presents a new concept for UFs and the subsequent subdivision led to new TDIs, based on the appropriate NOAEL or $BMDL_{05}$ derived from the reevaluation of available toxicity studies, and measured boron clearance and GFR used to derive them (Table 6). TDIs calculated from rat or dog studies were very similar, specifically, 0.26 and 0.22 mg B/kg/day, respectively. TDIs for developmental toxicity in mice and rats were also very similar, specifically 0.18 and 0.13 mg B/kg/day, and lower than TDIs for testicular toxicity. At this moment, it is considered that this is the best approach based on the latest scientific concept of uncertainty factors. In conclusion, the overall TDI of boron is 0.13 mg B/kg/day, based on a $BMDL_{05}$ from rat developmental toxicity and the scientifically developed uncertainty factors.

Conflict of interest statement

The authors declare that there are no conflicts of interest.

Acknowledgments

This work was supported by a Health and Labour Sciences Research Grant (H22-Kenki-Ippan-006) from the Ministry of Health, Labour and Welfare, Japan.

References

Allen, B.C., Strong, P.L., Price, C.J., Hubbard, S.A., Daston, G.P., 1996. Benchmark dose analysis of developmental toxicity in rats exposed to boric acid. Fundam. Appl. Toxicol. 32, 194–204.

Chapin, R., Dourson, M., Gomes, J., Hales, B., submitted for publication. Boric acid and its salts: third party review. Pesticide Management Regulatory Authority (PMRA) of Health Canada.

Connelly, J.C., Hasegawa, R., McArdle, J.V., Tucker, M.L., 1997. ICH guideline residual solvents. Pharmaeuropa 9 (Suppl. 1), S1–S68.

Dieter, M.P., 1994. Toxicity and carcinogenicity studies of boric acid in male and female B6C3F1 mice. Environ. Health Perspect. 102 (Suppl. 7), 93–97.

Dourson, M., Maier, A., Meek, B., Renwick, A., Ohanian, E., Poirier, K., 1998. Boron tolerable intake: re-evaluation of toxicokinetics for data-derived uncertainty factors. Biol. Trace Elem. Res. 66, 453–463.

Dourson, M.L., Stara, J.F., 1983. Regulatory history and experimental support of uncertainty (safety) factors. Regul. Toxicol. Pharmacol. 3, 224–238.

Duydu, Y., Başaran, N., Üstündağ, A., Aydin, S., Ündeğer, Ü., Ataman, O.Y., Aydos, K., Düker, Y., Ickstadt, K., Waltrup, B.S., Golka, K., Bolt, H.M., 2011. Reproductive toxicity parameters and biological monitoring in occupationally and environmentally boron-exposed persons in Bandirma, Turkey. Arch. Toxicol. 85, 589–600.

Dunlop, W., 1981. Serial changes in renal haemodynamics during normal human pregnancy. Br. J. Obstet. Gynaecol. 88, 1–9.
EFSA, 2004. Opinion of the scientific panel on dietetic products, nutrition and allergies on a request from the commission related to the tolerable upper intake level of boron (sodium borate and boric acid). EFSA J. 80, 1–22.
Falk-Filipsson, A., Hanberg, A., Victorin, K., Warholm, M., Wallen, M., 2007. Assessment factors–applications in health risk assessment of chemicals. Environ. Res. 104, 108–127.
Freireich, E.J., Gehan, E.A., Rall, D.P., Schmidt, L.H., Skipper, H.E., 1966. Quantitative comparison of toxicity of anticancer agents in mouse, rat, hamster, dog, monkey, and man. Cancer Chemother. Rep. 50, 219–244.
Hasegawa, R., Hirata-Koizumi, M., Dourson, M., Parker, A., Hirose, A., Nakai, S., Kamata, E., Ema, M., 2007. Pediatric susceptibility to 18 industrial chemicals: a comparative analysis of newborn with young animals. Regul. Toxicol. Pharmacol. 47, 296–307.
Hasegawa, R., Hirata-Koizumi, M., Dourson, M.L., Parker, A., Sweeney, L.M., Nishikawa, A., Yoshida, M., Ono, A., Hirose, A., 2010. Proposal of new uncertainty factor application to derive tolerable daily intake. Regul. Toxicol. Pharmacol. 58, 237–242.
Heindel, J.J., Price, C.J., Field, E.A., Marr, M.C., Myers, C.B., Morrissey, R.E., Schwetz, B.A., 1992. Developmental toxicity of boric acid in mice and rats. Fundam. Appl. Toxicol. 18, 266–277.
IPCS (International Programme on Chemical Safety), 1994. Assessing Human Health Risks of Chemicals: Derivation of Guidance Values for Health-Based Exposure Limits, Environmental Health Criteria, No. 170. World Health Organization, Geneva.
Jansen, J.A., Andersen, J., Schou, J.S., 1984. Boric acid single dose pharmacokinetics after intravenous administration to man. Arch. Toxicol. 55, 64–67.
Krutzen, E., Olofsson, P., Back, S.E., Nilsson-Ehle, P., 1992. Glomerular filtration rate in pregnancy: a study in normal subjects and in patients with hypertension, preeclampsia and diabetes. Scand. J. Clin. Lab. Invest. 52, 387–392.
Ku, W.W., Chapin, R.E., Moseman, R.F., Brink, R.E., Pierce, K.D., Adams, K.Y., 1991. Tissue disposition of boron in male Fischer rats. Toxicol. Appl. Pharmacol. 111, 145–151.
Lee, I.P., Sherins, R.J., Dixon, R.L., 1978. Evidence for induction of germinal aplasia in male rats by environmental exposure to boron. Toxicol. Appl. Pharmacol. 45, 577–590.
Lehman, A.J., Fitzhugh, O.G., 1954. 100-fold margin of safety. Assoc. Food Drug Off. US Quant. Bull. 18, 33–35.
Meek, M.E., Newhook, R., Liteplo, R.G., Armstrong, A.C., 1994. Approach to assessment of risk to human health for priority substances under the Canadian environmental protection act. J. Environ. Sci. Health C Environ. Carcinog. Ecotoxicol. Rev. 12, 105–134.
NTP (National Toxicology Program), 1987. Toxicology and carcinogenesis studies of boric acid (CAS No. 10043-35-3) in B6C3F1 mice (food studies). NTP Technical Report Series No. 324.
Pahl, M.V., Culver, B.D., Strong, P.L., Murray, F.J., Vaziri, N.D., 2001. The effect of pregnancy on renal clearance of boron in humans: a study based on normal dietary intake of boron. Toxicol. Sci. 60, 252–256.
Price, C.J., Marr, M.C., Myers, C.B., Seely, J.C., Heindel, J.J., Schwetz, B.A., 1996a. The developmental toxicity of boric acid in rabbits. Fundam. Appl. Toxicol. 34, 176–187.
Price, C.J., Strong, P.L., Marr, M.C., Myers, C.B., Murray, F.J., 1996b. Developmental toxicity NOAEL and postnatal recovery in rats fed boric acid during gestation. Fundam. Appl. Toxicol. 32, 179–193.
Renwick, A.G., 1993. Data-derived safety factors for the evaluation of food additives and environmental contaminants. Food Addit. Contam. 10, 275–305.
Robbins, W.A., Xun, L., Jia, J., Kennedy, N., Elashoff, D.A., Ping, L., 2010. Chronic boron exposure and human semen parameters. Reprod. Toxicol. 29, 184–190.
Sayli, B.S., 2001. Assessment of fertility and infertility in boron-exposed Turkish subpopulations. 3. Evaluation of fertility among sibs and in "borate families". Biol. Trace Elem. Res. 81, 255–267.
Sayli, B.S., 2003. Low frequency of infertility among workers in a borate processing facility. Biol. Trace Elem. Res. 93, 19–29.
Schneider, K., Oltmanns, J., Hassauer, M., 2004. Allometric principles for interspecies extrapolation in toxicological risk assessment–empirical investigations. Regul. Toxicol. Pharmacol. 39, 334–347.
Schou, J.S., Jansen, J.A., Aggerbeck, B., 1984. Human pharmacokinetics and safety of boric acid. Arch. Toxicol. Suppl. 7, 232–235.
Sturgiss, S.N., Wilkinson, R., Davison, J.M., 1996. Renal reserve during human pregnancy. Am. J. Physiol. 271, F16–F20.
Treinen, K.A., Chapin, R.E., 1991. Development of testicular lesions in F344 rats after treatment with boric acid. Toxicol. Appl. Pharmacol. 107, 325–335.
US Borax, 2000. UCI Boric acid clearance study reports and associated data: rat and human studies, April 4, 2000.
US EPA, 2004. Toxicological review of boron and compounds (CAS No. 7440-42-8) in support of summary information on the Integrated Risk, Information System (IRIS), US EPA.
US IOM, 2001. Dietary reference intakes for vitamin A, vitamin K, arsenic, boron, chromium, copper, iodine, iron, manganese, molybdenum, nickel, silicon, vanadium, and zinc. National Academy Press, Washington, DC.
Usuda, K., Kono, K., Orita, Y., Dote, T., Iguchi, K., Nishiura, H., Tominaga, M., Tagawa, T., Goto, E., Shirai, Y., 1998. Serum and urinary boron levels in rats after single administration of sodium tetraborate. Arch. Toxicol. 72, 468–474.
Vanderpool, R.A., Hof, D., Johnson, P.E., 1994. Use of inductively coupled plasma-mass spectrometry in boron-10 stable isotope experiments with plans, rats, and humans. Environ. Health Perspect. 102 (Suppl. 7), 13–20.
Vaziri, N.D., Oveisi, F., Culver, B.D., Pahl, M.V., Andersen, M.E., Strong, P.L., Murray, F.J., 2001. The effect of pregnancy on renal clearance of boron in rats given boric acid orally. Toxicol. Sci. 60, 257–263.
Weir Jr., R.J., Fisher, R.S., 1972. Toxicologic studies on borax and boric acid. Toxicol. Appl. Pharmacol. 23, 351–364.
WHO, 2005. Harmonization Project Document No. 2: Chemical-Specific Adjustment Factors for Interspecies Differences and Human Variability: Guidance Document for use of Data in Dose/Concentration-Response Assessment. World Health Organization, Geneva.
WHO, 2009. Boron in Drinking-Water, Background Document for Development of WHO Guidelines for Drinking-Water Quality. World Health Organization, Geneva.
Whorton, M.D., Haas, J.L., Trent, L., Wong, O., 1994. Reproductive effects of sodium borates on male employees: birth rate assessment. Occup. Environ. Med. 51, 761–767.
Yazbeck, C., Kloppmann, W., Cottier, R., Sahuquillo, J., Debotte, G., Huel, G., 2005. Health impact evaluation of boron in drinking water: a geographical risk assessment in Northern France. Environ. Geochem. Health 27, 419–427.

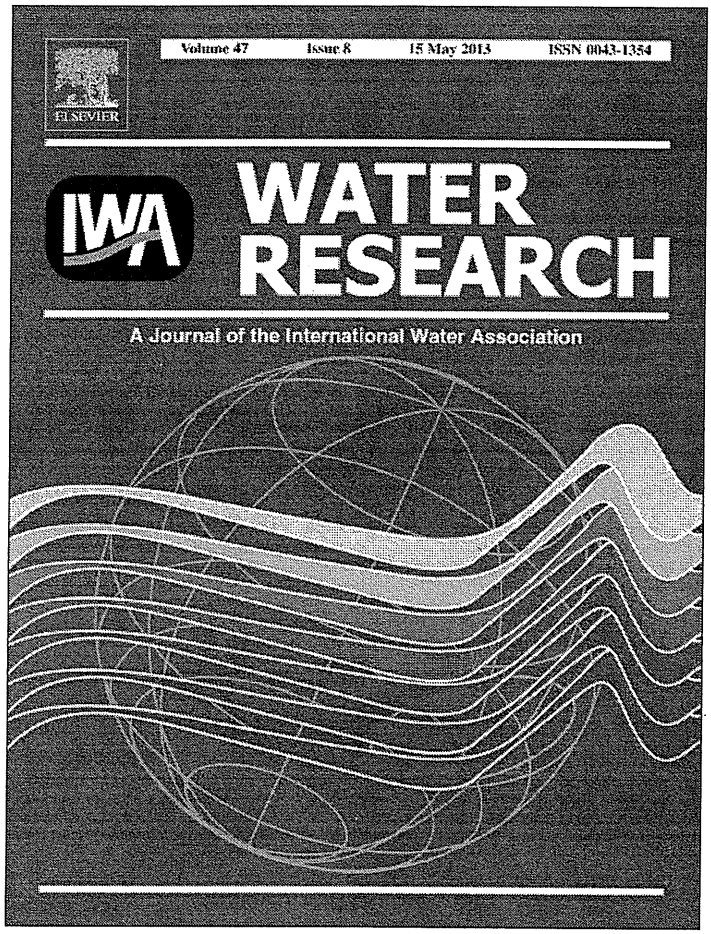

WATER RESEARCH 47 (2013) 2873–2880

Available online at www.sciencedirect.com

SciVerse ScienceDirect

journal homepage: www.elsevier.com/locate/watres

Geosmin and 2-methylisoborneol removal using superfine powdered activated carbon: Shell adsorption and branched-pore kinetic model analysis and optimal particle size

Yoshihiko Matsui [a,*], *Soichi Nakao* [b], *Takuma Taniguchi* [b], *Taku Matsushita* [a]

[a] *Faculty of Engineering, Hokkaido University, N13W8, Sapporo 060-8628, Japan*
[b] *Graduate School of Engineering, Hokkaido University, N13W8, Sapporo 060-8628, Japan*

ARTICLE INFO

Article history:
Received 19 July 2012
Received in revised form
18 February 2013
Accepted 23 February 2013
Available online 13 March 2013

Keywords:
Taste and odor
Water treatment
PAC
SPAC
Contact time

ABSTRACT

2-Methylisoborneol (MIB) and geosmin are naturally occurring compounds responsible for musty-earthy taste and odor in public drinking-water supplies, a severe problem faced by many utilities throughout the world. In this study, we investigated adsorptive removal of these compounds by superfine powdered activation carbon (SPAC, particle size <1 μm) produced by novel micro-grinding of powdered activated carbon; we also discuss the optimization of carbon particle size to efficiently enhance the adsorptive removal. After grinding, the absorptive capacity remained unchanged for a 2007 carbon sample and was increased for a 2010 carbon sample; the capacity increase was quantitatively described by the shell adsorption model, in which MIB and geosmin adsorbed more in the exterior of a carbon particle than in the center. The extremely high uptake rates of MIB and geosmin by SPAC were simulated well by a combination of the branched-pore kinetic model and the shell adsorption model, in which intraparticle diffusion through macropores was followed by diffusion from macropore to micropore. Simulations suggested that D_{40} was on the whole the best characteristic diameter to represent a size-disperse group of adsorbent particles; D_{40} is the diameter through which 40% of the particles by volume pass. Therefore, D_{40} can be used as an index for evaluating the improvement of adsorptive removal that resulted from pulverization. The dose required for a certain percentage removal of MIB or geosmin decreased linearly with carbon particle size (D_{40}), but the dose reduction became less effective as the activated carbon was ground down to smaller sizes around a critical value of D_{40}. For a 60-min contact time, critical D_{40} was 2–2.5 μm for MIB and 0.4–0.5 μm for geosmin. The smaller critical D_{40} was when the shorter the carbon–water contact time was or the slower the intraparticle mass transfer rate of an adsorbate was.

1. Introduction

For drinking water suppliers, removing any objectionable tastes and odors is key to ensuring customer satisfaction. Two important compounds, geosmin and 2-methylisoborneol (MIB), impart a strong musty-earthy taste and odor that lead to customer complaints even at concentrations as low as 10 ng/L. These compounds are the metabolites of various microorganisms, including cyanobacteria. Japan's drinking water quality standard regulates geosmin and MIB concentrations in tap water to be lower than 10 ng/L each; this is the lowest concentration level among other constituents. Effective and accepted treatment options to control taste and odor compounds include ozone oxidation and adsorption using

* *Corresponding author*. Tel./fax: +81 11 706 7280.
E-mail address: matsui@eng.hokudai.ac.jp (Y. Matsui).
0043-1354/$ – see front matter © 2013 Elsevier Ltd. All rights reserved.
http://dx.doi.org/10.1016/j.watres.2013.02.046

granular or powdered activated carbon (PAC). Among these options, PAC treatment is the simplest method and perhaps the most widely applied (e.g., Srinivasan and Sorial, 2011), but is rather expensive compared to conventional treatment processes such as coagulation treatment, in particular when it is used on a continuous basis. A key difficulty with PAC is that the adsorption of MIB and geosmin is relatively slow. A very long PAC–water contact time is essential to utilize the PAC's full adsorptive capacity (Huang et al., 1996; Gillogly et al., 1998; Cook et al., 2001); alternatively, a higher dose of PAC can be used, but this increases treatment cost.

PAC's effectiveness as an adsorbent is influenced by various characteristics, including its surface chemistry, pore structure, and particle size. Micropore volume and oxygen content are key properties affecting the equilibrium adsorption capacity of activated carbon (Pendleton et al., 1997; Considine et al., 2001; Nowack et al., 2004; Yu et al., 2007; Tennant and Mazyck, 2007). Besides equilibrium capacity, adsorption kinetics is another important aspect of adsorptive removal, and smaller adsorbent particles have faster adsorption kinetics (e.g., Najm et al., 1990). Accordingly, reducing particle size to improve PAC's adsorbate uptake rate is one measure to more efficiently utilize its adsorptive capacity. Although adsorption kinetics can be enhanced by reducing the activated carbon particle size, the overall adsorption capacity is unaffected by particle size because adsorption occurs in the internal pores of the activated carbon particles (Letterman et al., 1974; Peel and Benedek, 1980; Leenheer, 2007). However, the recent advent of superfine powdered activated carbon (SPAC) has renewed discussions on the relationship between particle size and adsorption capacity as well as it has prompted new discussions on the relationship in the sub-micron domain (Matsui et al., 2004, 2005; Heijman et al., 2009). Smaller activated carbon particles have been reported to have greater adsorption capacity for some macromolecules, including natural organic matter (NOM); the dependency of adsorption capacity on adsorbent size is well described by the shell adsorption model (SAM; Ando et al., 2010; Matsui et al., 2011). SPAC is also superior to PAC in removing geosmin and mitigating membrane fouling when it is used in adsorption pretreatment before microfiltration (Matsui et al., 2007, 2009b; Huang et al., 2009).

The homogeneous surface diffusion model (HSDM) has traditionally been used to predict the effect of adsorbent particle size on kinetics (Huang et al., 1996; Cook et al., 2001; Newcombe and Cook, 2002). However, HSDM does not accurately describe geosmin adsorption on adsorbents of different particle sizes, such as SPAC and PAC, unless the model is modified to vary surface diffusivity according to changes in carbon particle size (Matsui et al., 2009a). Therefore, HSDM does not truly predict the effect of carbon particle size on adsorptive removal. The branched-pore kinetic model (BPKM), which consists of macropore diffusion followed by mass transfer from macropore to micropore, accurately describes the adsorption kinetics on SPAC and PAC with the same set of model parameter values, including surface diffusivity. In a previous study (Matsui et al., 2009a), BPKM was used in conjunction with the Freundlich isotherm equation, and the adsorption isotherms of SPAC and PAC were assumed to be the same. However, the use of BPKM to model adsorption kinetics on the assumption that the adsorption capacities of SPAC and PAC are different has not been tested. Moreover, BPKM has not been applied to the removal of MIB or MIB/geosmin in natural water systems. The relationship between MIB and geosmin removal rates and adsorbent particle size has not yet been fully analyzed, particularly in the micron and submicron range.

In the present study, we performed adsorption equilibrium and kinetics experiments to assess the capacity and the rate of MIB and geosmin uptake onto SPAC and PAC, both in the presence of NOM and in single-solute systems. To consider the effects of carbon particle size on both adsorption capacity and kinetics, we applied BPKM in conjunction with SAM. In this paper we discuss the effects of activated carbon particle size, as well as optimum particle size.

2. Materials and methods

2.1. Activated carbon

Commercially available wood-based PAC (Taikou-W, Futamura Chemical Industries Co., Gifu, Japan) was obtained in the years 2007 and 2010. SPAC was prepared by pulverizing PAC in a wet bead mill (Metawater Co., Tokyo, Japan). Both PAC and SPAC samples were slurried in ultrapure water and were stored at 4 °C. In this paper, we refer to the as-received PAC obtained in 2007 as PAC07 and that obtained in 2010 as PAC10. The pulverized carbons are referred to similarly as SPAC07 and SPAC10. We also prepared another set of pulverized carbons with median diameters between those of PAC and SPAC; these are referred to as SPACb07 and SPACb10. Particle size distributions of the activated carbon samples were determined using a laser-light scattering instrument (LA-700, Horiba, Kyoto, Japan); the samples were prepared for analysis by suspension of SPAC/PAC in water to make 200-mL samples containing 0.001–0.01% carbon, followed by addition of a dispersant (0.02 mL of an 18% solution of anionic surfactant) and ultrasonication for 4 min Table 1 summarizes the properties of each activated carbon.

2.2. Water samples

Water containing NOM was collected from Lake Hakucho, Hokkaido, Japan. The sample was transported in polyethylene tanks and stored at 4 °C. The water was filtered through a 0.2-μm-pore membrane (DISMIC-25HP; Toyo Roshi Kaisha, Tokyo) and diluted to adjust the dissolved organic carbon concentration to ~1.5 mg/L; the diluent used for this purpose was prepared by amending ultrapure water (Milli-Q Advantage, Millipore Co.) with salts to obtain an ionic composition similar to that used in a previous study (Matsui et al., 2012). Stock solutions of MIB and geosmin were prepared by dissolving the pure chemicals (Wako Pure Chemical Industries, Osaka, Japan) in ultrapure water. The dissolution was confirmed by 0.2-μm membrane filtering. The NOM-containing waters (NOMWs) were spiked with the MIB or geosmin stock solutions to prepare samples with an initial MIB or geosmin concentration of ~1 μg/L. For single-solute MIB and geosmin experiments, the MIB or geosmin stock solution was added to ultrapure water amended with inorganic ions such that the ionic composition was similar to that of the NOMW; we refer to this water as organic-free water (OFW). All water samples were filtered

Table 1 – Size and surface area characteristics of the activated carbon particles studied.

Sample name	Median diameter (D_{50}, μm)	Effective diameter (D_{10}, μm)	Uniformity coefficient	Geometric standard deviation	BET surface area (m^2/g)
PAC07	11.8	3.89	3.27	2.27	1170
SPACb07	1.91	0.904	2.34	1.85	n/a
SPAC07	0.725	0.271	3.15	1.93	1110
PAC10	13.5	3.35	5.19	2.80	1070
SPACb10	4.87	0.853	7.59	3.29	n/a
SPAC10	0.857	0.396	2.70	3.00	1130

through a 0.2-μm-pore membrane before use. MIB and geosmin concentrations were analyzed using a purge-and-trap concentrator coupled to a gas chromatograph equipped with a mass spectrometer (GCMS-QP2010 Plus; Shimadzu Corp., Kyoto, Japan; Aqua PT 5000 J, GL Sciences Inc., Tokyo, Japan). Dissolved organic carbon was quantified using a Model 810 carbon analyzer (Sievers Instruments, Inc., Boulder, CO, USA).

2.3. Batch adsorption tests

In adsorption equilibrium tests, 150-mL aliquots of OFW or NOMW spiked with MIB or geosmin ($C_0 = \sim 1$ μg/L) were transferred to 160-mL vials. A specified amount of SPAC/PAC was immediately added, the vials were manually shaken, and then the samples were agitated on a mechanical shaker for one week at a constant temperature of 20 °C. In a preliminary experiment, it was confirmed that MIB and geosmin adsorption equilibriums were reached within one week and that NOM adsorption nearly reached equilibrium. Several bottles that did not contain PAC or SPAC were used as control samples to confirm that the concentrations of MIB, geosmin, and NOM changed negligibly during long-term agitation. After water samples were filtered through a 0.2-μm-pore membrane filter, the MIB and geosmin concentrations in the aqueous phase were measured. Solid-phase concentrations of each adsorbate were calculated from the mass that remained in the aqueous phase.

Adsorption kinetics was investigated with sample waters (3 L or 1 L) each containing MIB or geosmin ($C_0 = \sim 1$ μg/L) in a beaker with efficient mixing (200 rpm). After the addition of a specified amount of activated carbon suspension, aliquots were withdrawn at intervals and filtered immediately through a 0.2-μm-pore membrane filter for analysis of the aqueous MIB and geosmin concentrations.

3. Results and discussion

3.1. Equilibrium and kinetics of adsorption

Adsorption equilibrium tests were conducted for MIB and geosmin in the OFW system to compare SPAC with PAC. SPAC07 and SPACb07 had slightly greater MIB adsorption capacity than PAC07, but the difference (11%) was very small (Fig. 1A). This result suggests that grinding did not effectively increase the MIB adsorption capacity of PAC07. SPAC10 and

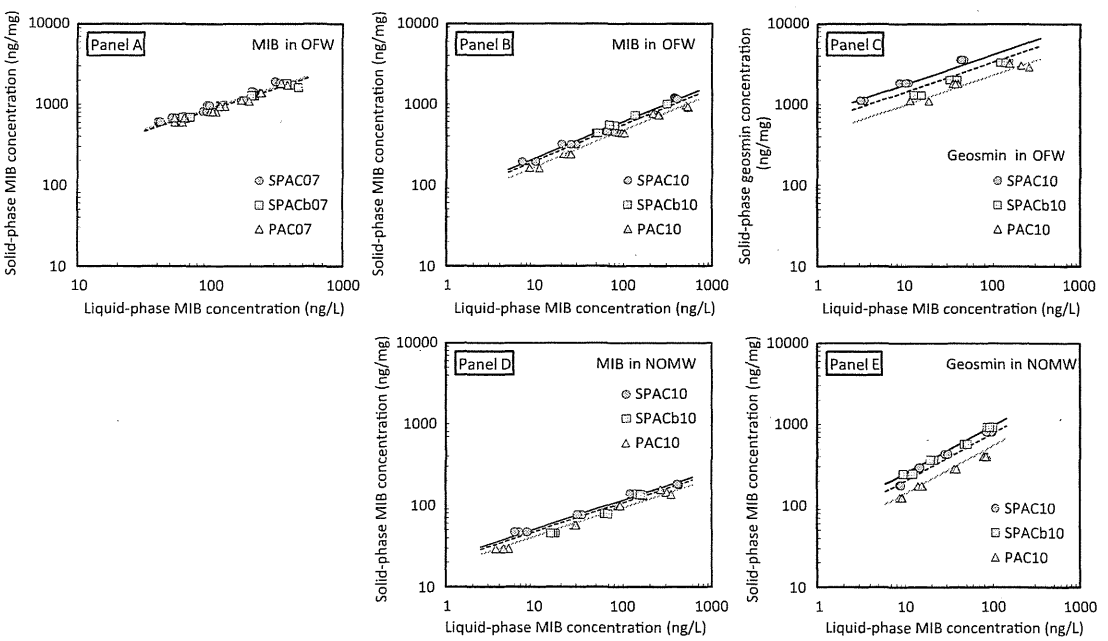

Fig. 1 – Adsorption isotherms for MIB (Panels A, B, and D) and geosmin (Panels C and E). Experimental data are shown as points, and SAM fits to the data are shown as lines. The SAM fit parameters are as follows: Panel A–K_0: 3.1 (mg/g)/(ng/L)$^{1/n}$, δ: 38.6, 1/n: 0.54. Panel B–K_0: 1.8 (mg/g)/(ng/L)$^{1/n}$, δ: 9.1, 1/n: 0.46. Panel C–K_0: 10.7 (mg/g)/(ng/L)$^{1/n}$, δ: 3.0, 1/n: 0.37. Panel D–K_0: 0.3 (mg/g)/(ng/L)$^{1/n}$, δ: 11.0, 1/n: 0.36. Panel E–K_0: 4.1 (mg/g)/(ng/L)$^{1/n}$, δ: 3.2, 1/n: 0.59.

SPACb10 showed a somewhat greater increase in MIB adsorption capacity relative to that of PAC10; the capacity of SPAC10 was 27% greater than that of PAC10 (Fig. 1B). For geosmin, the adsorption capacity difference was more pronounced, with the clear trend SPAC10 > SPACb10 > PAC10 (Fig. 1C). We also conducted adsorption equilibrium tests by using natural water spiked with MIB or geosmin to elucidate the superiority of SPAC over PAC for removing MIB and geosmin under the influence of NOM. Adsorption isotherms of MIB in the presence of NOM show that SPAC10 had 23% more MIB adsorption capacity than PAC10 under this condition. The presence of NOM reduced the MIB adsorption capacity on SPAC by 85% while it reduced the capacity on PAC by 84% indicating that the adsorption capacities of SPAC and PAC were reduced to a similar extent by competitive adsorption of NOM (Fig. 1D). The same influence of NOM on the adsorption capacity between SPAC and PAC suggests the same loading of NOM that compete with MIB for adsorption sites. Details for the effect of NOM loading on SPAC and PAC adsorption are seen elsewhere (Matsui et al., 2012). The presence of NOM also reduced the geosmin adsorption capacities of SPAC and PAC to a similar extent (Fig. 1E); as with MIB, the geosmin adsorption capacity of SPAC10 in the presence of NOM was also higher than that of PAC10.

The phenomenon that grinding carbon particles to reduce their size increased adsorption capacity is explained by means of a mechanism whereby molecules do not completely penetrate the adsorbent particle and instead preferentially adsorb near the outer surface of the particle (Ando et al., 2010), and the observed changes in adsorption isotherms according to carbon particle size are described well by SAM (see lines in Fig. 1; see also Matsui et al., 2011), which was originally developed to describe the adsorption of NOM. In SAM, the adsorption capacity parameter, that is, the Freundlich K value, decreases linearly with distance from the external surface to a certain depth:

$$K_S(r,R) = K_0 \left[\max\left(\frac{r-R+\delta}{\delta}, 0\right)\right] \quad (1)$$

where r is the radial distance from the center of an adsorbent particle (cm), R is the adsorbent particle radius (cm); $K_S(r, R)$ is the Freundlich adsorption capacity parameter ((ng/mg)/(ng/L)$^{1/n}$), which varies as a function of radial distance r and adsorbent radius R; K_0 is the Freundlich parameter of adsorption at the external adsorbent particle surface ((ng/mg)/(ng/L)$^{1/n}$); δ is the penetration depth, or in other words the thickness of the penetration shell (cm); and n is the dimensionless Freundlich exponent.

In contrast to the adsorption equilibria, the adsorption kinetics of SPAC and PAC were extremely different: SPAC had a much faster uptake rate than PAC under every condition studied (Fig. 2). In both OFW and NOMW systems, uptake rates of geosmin and MIB were improved greatly by using SPAC. For example, a 0.5 mg/L dose of SPAC removed geosmin at almost the same rate as 3 mg/L of PAC (Fig. 2C). PAC would show little removal if the dosage was 0.5 mg/L, that was the same as that of SPAC, but this experiment was not conducted because the objective of the experiments was model parameter determination, where the data of little removal was ineffective.

These experimental data of adsorption kinetics were simulated by applying BPKM (Matsui et al., 2009a), modified by incorporating SAM to describe the local adsorption equilibria in internal pores of the carbon particle. The original BPKM assumes radial intraparticle diffusion through macropores in an adsorbed state (surface diffusion). However, the surface diffusion scenario could not be applied in this study, because it assumes that the interior of the activated carbon particle is homogeneous. Such homogeneity implies that adsorbed

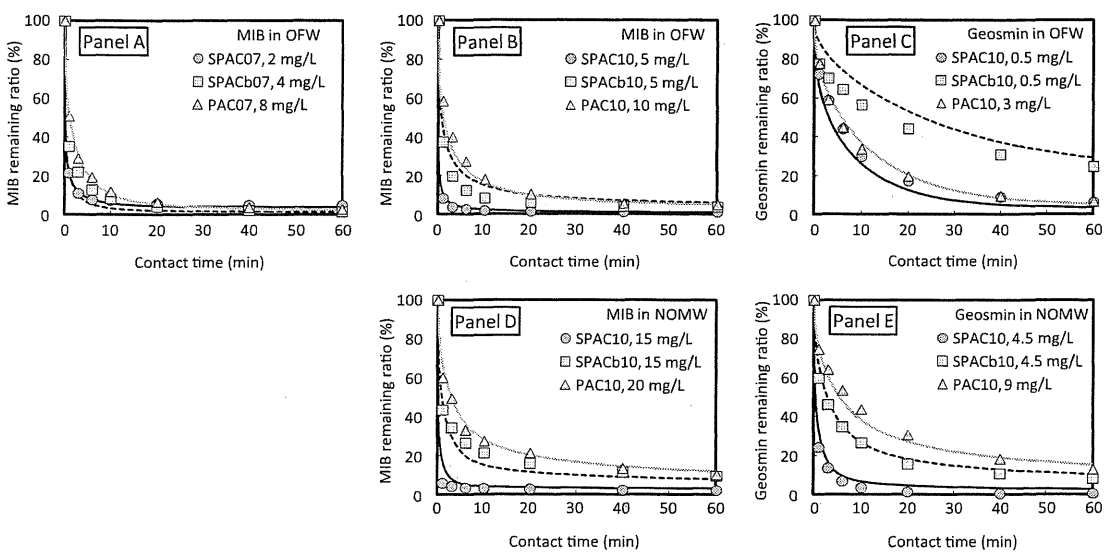

Fig. 2 – Adsorption kinetics for MIB (Panels A, B, and D) and geosmin (Panels C and E). Experimental data are shown as points, and BPKM-SAM simulations are shown as lines. Initial MIB and geosmin concentrations are ~1 μg/L. The BPKM-SAM parameters are as follows: Panel A – D_P: 1.7 × 10^{-7} cm^2/s, K_S: 8.7 × 10^{-4} s^{-1}, ϕ: 0.57. Panel B – D_P: 3.1 × 10^{-7} cm^2/s, K_S: 3.9 × 10^{-4} s^{-1}, ϕ: 0.73. Panel C – D_P: 2.1 × 10^{-7} cm^2/s, K_S: 3.8 × 10^{-4} s^{-1}, ϕ: 0.29. Panel D – D_P: 3.0 × 10^{-7} cm^2/s, K_S: 2.1 × 10^{-3} s^{-1}, ϕ: 0.55. Panel E – D_P: 0.44 × 10^{-7} cm^2/s, K_S: 1.5 × 10^{-3} s^{-1}, ϕ: 0.53.

molecules have migrated into adsorbent particles by Fick's first law of diffusion according to a local solid-phase concentration gradient, and that adsorbate molecules are ultimately distributed evenly across the inside surface of an adsorbent such that local solid-phase concentrations become equal. Such a scenario is inconsistent with SAM. Therefore, instead of modeling diffusion in an adsorbed state, we modeled diffusion of molecules in liquid-filled macropores (pore diffusion). Mass transfer resistance across the liquid film external to adsorbent particle surfaces was substantially neglected by giving a large value (10 cm/s) of liquid film mass transfer coefficient because it cannot be the rate-determining step in well mixed reactors (Sontheimer et al., 1988; Matsui et al., 2009a).

Finally, the macropore mass balance equation is as follows:

$$\phi\frac{\partial q_M(t,r,R)}{\partial t}=\frac{\varnothing D_P}{\rho r^2}\frac{\partial}{\partial r}\left(r^2\frac{\partial c_M(t,r,R)}{\partial r}\right)-k_B\left[q_M(t,r,R)-q_B(t,r,R)\right] \quad (2)$$

where t is adsorption time in the batch system (s); ϕ is the fraction of adsorptive capacity available in the macropore region (dimensionless); ρ is the adsorbent particle's density (g/L); D_P is the diffusion coefficient in the macropore (cm^2/s); c_M (t, r, R) is the liquid-phase concentration in a macropore of an adsorbent of radius R, at radial distance r and time t (ng/L); q_M (t, r, R) is the solid-phase concentration in a macropore of an adsorbent of radius R, at radial distance r and time t (ng/g); q_B (t, r, R) is the solid-phase concentration in a micropore of an adsorbent of radius R, at radial distance r and time t (ng/g); and k_B is the rate coefficient for mass transfer between macropores and micropores (s^{-1}).

The local adsorption equilibrium is expressed as follows:

$$c_M(t,r,R)=\left(\frac{q_M(t,r,R)}{K_S(r,R)}\right)^n \quad (3)$$

The other BPKM equations can be seen elsewhere (Matsui et al., 2009a).

Model simulations of both MIB and geosmin concentrations were overall successful in describing the curves of concentration vs. contact time in a batch adsorption system (see the lines in Fig. 2). Therefore, once the adsorption equilibrium and kinetic model parameters are determined, one can predict the MIB and geosmin concentrations at a given carbon–water contact time and a given carbon particle size distribution. Using this model, one can evaluate the effect of carbon particle size on the concentrations of MIB and geosmin remaining after a given contact time.

3.2. *Representative diameter for adsorption kinetics*

With the successful application of BPKM-SAM to MIB and geosmin adsorption in OFW and NOMW systems, it becomes possible to quantitatively evaluate the optimum adsorbent diameters for MIB and geosmin removal. A complicating factor in studying adsorption is that activated carbon products typically consist of particles with a wide size distribution, and the dispersity of this distribution also varies considerably among different products and preparations. Therefore, we first investigated a characteristic particle size that would best represent the entire size distribution of any given carbon sample. If a suitable definition of characteristic size can be found, this greatly simplifies the problem and allows us to understand the group's adsorption kinetics using a single size value (Traegner et al., 1996). Such a characteristic size should be a measure of central tendency, which is unaffected by the relatively few extreme values in the tails of the distribution. We tested several definitions of characteristic size: D_{20} (i.e., the diameter that 20% by volume of the all particles are finer than), D_{30}, D_{40}, D_{50}, and D_{60}. In selecting the best characteristic size, we created three fictitious particle size distributions (see Fig. 3): a uniform distribution (uniformity coefficient of 1.0), a moderate distribution with a uniformity coefficient of 2.34 (the value was taken from the actual particle size distribution of SPACb07), and a wider size distribution with a uniformity coefficient of 7.59 (the value was taken from SPACb10).

Using BPKM-SAM, we simulated geosmin concentration decay for the three adsorbents each having different particle size distributions but all having the same characteristic size. In the case of D_{40}, the three curves were not so different (Fig. 4), suggesting that the geosmin adsorption kinetics were almost the same among carbon samples whose D_{40} was the same, regardless of whether their particle size distribution was narrow or wide. The root mean square (RMS) of C/C_0 (remaining ratio) deviations between the moderate distribution with uniformity coefficient 2.34 and the wide distribution with 7.59 was 0.013, and the RMS value between the moderate distribution with 2.34 and the uniform distribution with 1.0 was 0.024. We conducted this kind of BPKM simulation for D_{20}, D_{30}, D_{40}, D_{50}, and D_{60}, for both MIB and geosmin and in both OFW and NOMW; for MIB removal, RMS was minimized using D_{40}, whereas D_{30} was optimal for geosmin (Fig. 5). Therefore, D_{40} was the best characteristic size to represent the kinetics of MIB removal (Fig. 5A), whereas D_{30} was the best for geosmin removal (Fig. 5B). We understand that for an adsorbate having a slow intraparticle mass transfer rate in a carbon particle, carbon fractions with small sizes, because they have relatively large external surface area, make a major contribution to adsorptive removal when contact times are limited. In such a

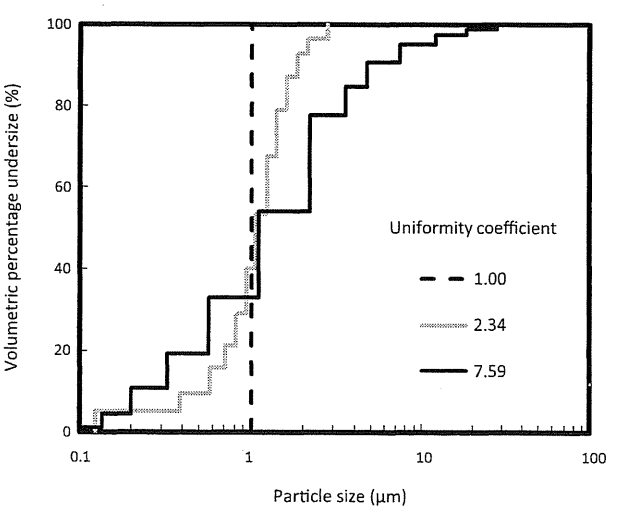

Fig. 3 – Fictitious adsorbent particle size distributions with the same D_{40} (1.0 μm) for BPKM-SAM simulations.